BNL-72286-2004

Computational Science Center

in affiliation with the Departments of

Applied Mathematics and Statistics and
Computer Science
Stony Brook University

www.bnl.gov/csc

November 2004

Brookhaven National Laboratory
P.O. Box 5000
Upton, NY 11973-5000
www.bnl.gov

Managed by
Brookhaven Science Associates, LLC
for the United States Department of Energy under
Contract No. DE-AC02-98CH10886

DISCLAIMER

FOR UNCLASSIFIED, UNLIMITED STI PRODUCTS

Available electronically at:

OSTI:
http://www.osti.gov/bridge

Available for a processing fee to U.S. Department of Energy and its contractors, in paper from:

U.S. Department of Energy
Office of Scientific and Technical Information
P.O. Box 62
Oak Ridge, TN 37831
Phone: (865) 576-8401
Facsimile: (865) 576-5728
E-mail: reports@adonis.osti.gov

National Technical Information Service (NTIS):

Available for sale to the public from:

U.S. Department of Commerce
National Technical Information Service
5285 Port Royal Road
Springfield, VA 22131
Phone: (800) 553-6847
Facsimile: (703) 605-6900
Online ordering: http://www.ntis.gov/ordering.htm

BROOKHAVEN COMPUTATIONAL SCIENCE CENTER

Page

1. INTRODUCTION

The Brookhaven Computational Science Center brings together researchers in biology, chemistry, physics, and medicine with applied mathematicians and computer scientists to exploit the remarkable opportunities for scientific discovery which have been enabled by modern computers.

These opportunities are especially great in computational biology and nanoscience, but extend throughout science and technology and include for example, nuclear and high energy physics, astrophysics, materials and chemical science, sustainable energy, environment, and homeland security.

To achieve our goals we have established a close alliance with applied mathematicians and computer scientists at Stony Brook and Columbia Universities.

2. OVERVIEW

Science has become increasingly dependent on computers and computing. New machines, with 100,000 processors or more have made possible the vision of simulation as the 'third tier' of science, on an equal footing with experiment and traditional theory. Many experiments produce so much data of such complexity that they require extensive data collection, storage and analysis capabilities in order to be successful.

In recognition of these trends, DOE's Office of Science has embarked on a long range program to upgrade the computing infrastructure within the Laboratory complex and to make the most advanced systems available to researchers throughout the scientific community.

Brookhaven currently has major efforts in data storage and analysis for the Relativistic Heavy Ion Collider (RHIC) and the ATLAS detector at CERN, and in quantum chromodynamics. We will serve as host for the QCDOC machines (quantum chromodynamics on a chip) 10 teraflop/s computers which boast more than 10,000 processors each. There will two here, one for the Riken/BNL Research Center and the other shared by the US Lattice Gauge Community and other scientific users.

Our Center for Data Intensive Computing, predecessor to CSC, has established a strong program in computational science, with an emphasis on nanoscale electronic structure and molecular dynamics, accelerator design, computational fluid dynamics, medical imaging, parallel computing and numerical algorithms. We have been an active participant in DOE's SciDAC program (Scientific Discovery through Advanced Computing).

In keeping with Laboratory initiatives we are planning a major expansion in computational biology and preparing for a large parallel machine such as IBM's BlueGene/L.

3. PERSONNEL

The Director of the Computational Science Center (CSC) is James Davenport; James Glimm is Head of Applied Mathematics, and the Administrative Assistant is Claire Lamberti. CSC is located in Building 463, Room 255, at Brookhaven National Laboratory, Upton NY 11973-5000.

CSC grew out of the Center for Data Intensive Computing, which was established in 1999. It currently has a staff of 14. As part of an active, ongoing collaboration with graduate students from Stony Brook, ten Ph.D. students and several undergraduates hold scientific positions in CSC.

TABLE 1. CSC STAFF

Name	Position	Phone/email
James Davenport	Director	631-344-3789 jdaven@bnl.gov
James Glimm	Head, Applied Mathematics	631-344-8155 glimm@bnl.gov
David Keyes	Visiting Scientist	631-344-5752
Nicholas D'Imperio	Physics Associate	631-344-8589 dimperio@bnl.gov
Stratos Efstathiadis	Technology Architect	631-344-6080 stratos@bnl.gov
Michael McGuigan	Computer Scientist	631-344-2695 mcguigan@bnl.gov
Wonho Oh	Assistant Scientist	631-344-8156 woh@bnl.gov
Roman Samulyak	Associate Scientist	631-344-3304 rosamu@bnl.gov
Leonard Slatest	Advanced Technology Engineer	631-344—4102 slatest@bnl.gov
Gordon Smith	Technology Architect	631-344-3216 smith3@bnl.gov
John Spiletic	Technology Architect	631-344-4112 spiletic@bnl.gov
David Stampf	Senior Technology Architect	631-344-4148 drs@bnl.gov
Robert Bennett	Research Associate	631-344-6080 robertb@bnl.gov
Kab Seok Kang	Research Associate	631-344-3580 kskang@bnl.gov
Myoung-Nyoun Kim	Research Associate	631-344-2089 mnkim@bnl.gov
Yarema Prykarpatskyy	Research Associate	631-344-8603 yarpry@bnl.gov
Zhiliang Zhu	Research Associate	631-344-3051
Jincheng Zheng	Research Associate	631-344-6351 jczheng@bnl.gov
Claire Lamberti	Administrative Assistant	631-344-3051 lamberti@bnl.gov

TABLE 2. CSC AFFILIATES		
Name	**Affiliation**	**Expertise**
Carl Anderson	BNL/Biology	Protein Structures
Carmen Benkovitz	BNL/Environmental Sciences	Atmospheric Transport
Helene Benveniste	BNL/Directorate	Neuroscience
Michael Creutz	BNL/Physics	Lattice Gauge Theory
Yuefan Deng	SB/Applied Math. & Statistics	Molecular Dynamics
Steven Evans	Beth Israel Medical Center	Cardiac Physiology
Flavio Fenton	Hofstra University	Cardiac Simulation
Erwin George	SB/Applied Math & Statistics	Fluid Dynamics
John Grove	Los Alamos National Lab.	Computational Science
Harold Hastings	Hofstra University	Dynamical Systems
Jiansheng Jiang	BNL/Biology	Protein Structures
Arie Kaufman	SB/Computer Science	Visualization
Jerome Lauret	BNL/Physics	Grid Computing
Xiaolin Li	SB/Applied Math. & Statistics	Computational Science
Brent Lindquist	SB/Applied Math. & Statistics	Porous Media; Image Analysis
Alfredo Luccio	BNL/AGS	Accelerator Design
Walter Mangel	BNL/Biology	Structural Biology
Edward McFadden	BNL/ITD	Parallel Hardware
James Muckerman	BNL/Chemistry	Combustion Chemistry
Klaus Mueller	SB/Computer Science	Visualization
Arnold Peskin	BNL/CSC & ITD	Visualization
John Pinezich	Advanced Acoustic Concepts	Computational Fluid Dynamics
Hong Qin	SB/Computer Science	Parallel Computing
Marwan Rasamny	Delaware State University	Computational Materials Science
John Reinitz	SB/Applied Math. & Statistics	Computational Biology
Robert Rizzo	SB/Applied Math. & Statistics	Computational Biology
Stephen Schwartz	BNL/Environmental Sciences	Aerosol and Climate Modeling
David Sharp	Los Alamos National Lab.	Computational Science
Carlos Simmerling	SB/Chemistry	Protein Structures
William Studier	BNL/Biology	Protein Structures
S. Swaminathan	BNL/Biology	Structural Biology
Michael Weinert	Univ. of Wisconsin/Milwaukee	Condensed Matter Physics
Torre Wenaus	BNL/Physics	High Energy and Nuclear Physics
Wei Zhu	SB/Applied Math. & Statistics	Statistics; Image Analysis

TABLE 3. STUDENT AFFILIATES	
Name	**Affiliation**
Serena Chan	Cornell/Statistics
Xin Chen	SB/Applied Mathematics & Statistics
Yongzhi Chen	SB/Applied Mathematics & Statistics
Srabasti Dutta	SB/Applied Mathematics & Statistics
Bin Fang	SB/Applied Mathematics & Statistics
Yuxiang Gao	SB/Applied Mathematics & Statistics
Youlia Guilman	SB/Physics
Guowen Han	SB/Applied Mathematics & Statistics
Tianshi Lu	SB/Applied Mathematics & Statistics tlu@ic.sunysb.edu
Nitin Pillai	SB/Applied Mathematics & Statistics
Tatiana Polischuk	SB/Applied Mathematics & Statistics
Peter Rissland	SB/ Applied Mathematics & Statistics rissland@ams.sunysb.edu
Julie Stern	SB/Chemistry
Tao Sun	SB/Applied Mathematics & Statistics
Dmitri Volja	SB/Physics dvolia@physics.sunysb.edu
Shuqiang Wang	SB/Applied Mathematics & Statistics
Xuena Wang	SB/Applied Mathematics & Statistics
Xiangfeng Wu	SB/Applied Mathematics & Statistics
Bin Xu	SB/Applied Mathematics & Statistics
Yue Zhang	SB/Applied Mathematics & Statistics

4. RESEARCH

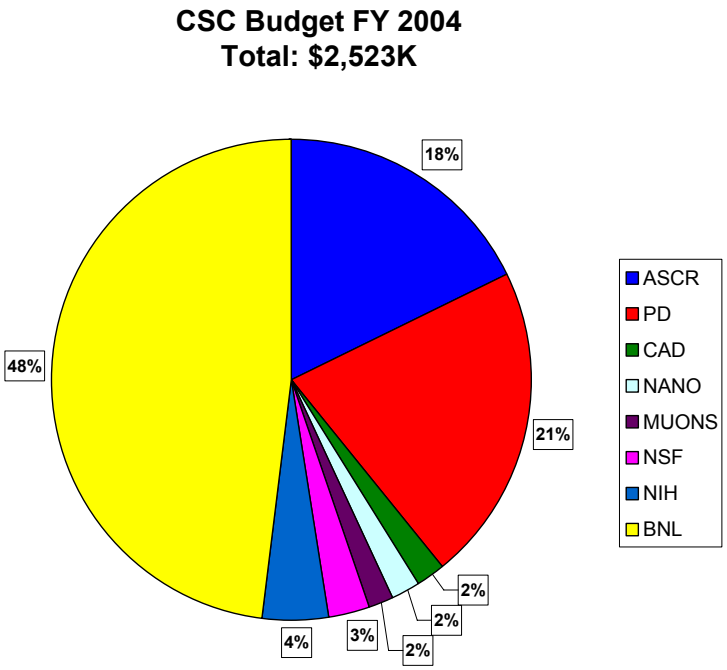
CSC Budget FY 2004
Total: $2,523K
18%
21%
2%
2%
2%
3%
4%
48%
ASCR
PD
CAD
NANO
MUONS
NSF
NIH
BNL

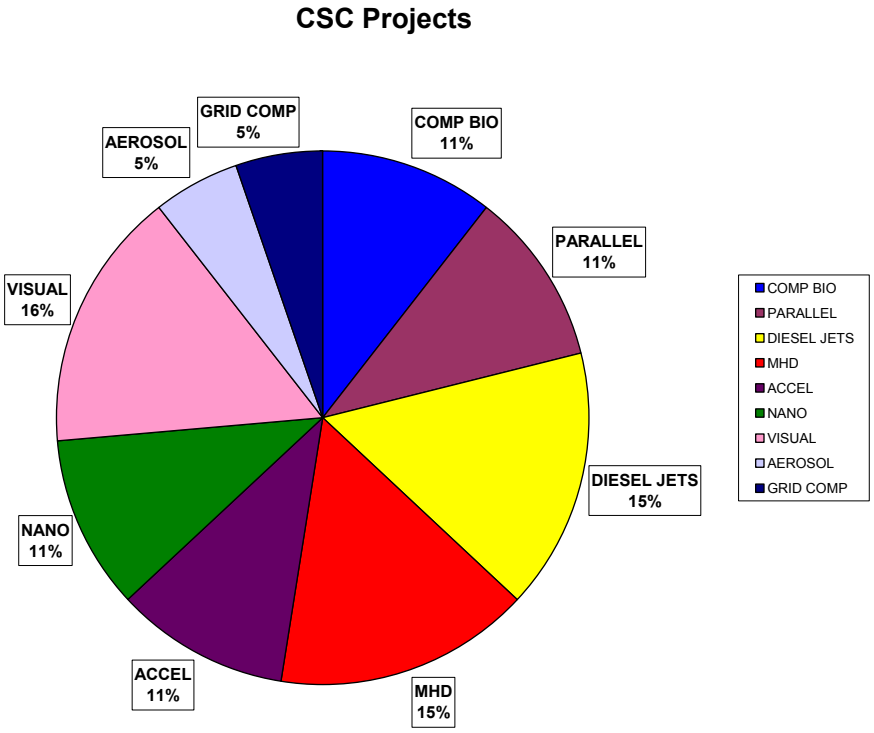
CSC Projects
COMP BIO 11%
PARALLEL 11%
DIESEL JETS 15%
MHD 15%
ACCEL 11%
NANO 11%
VISUAL 16%
AEROSOL 5%
GRID COMP 5%
COMP BIO
PARALLEL
DIESEL JETS
MHD
ACCEL
NANO
VISUAL
AEROSOL
GRID COMP

4.1 SciDAC at CSC

Scientific Discovery through Advanced Computing (SciDAC) is a five-year program to develop the Scientific Computing Software and Hardware Infrastructure to support terascale computations for DOE's research programs.

4.1.1 TSTT

J. Glimm, M.-N. Kim, and W. Oh

At Brookhaven we have formed an alliance with researchers at Argonne, Livermore, Oak Ridge, Pacific Northwest, Rensselaer, Sandia, and Stony Brook, to develop technologies that enable scientists to use complex mesh and discretization strategies easily, within a single simulation on terascale computers. The Terascale Simulation Tools and Technologies (TSTT) Center provides interoperable tools to facilitate use of advanced mesh and discretization technologies. The Center has developed standardized interfaces to local mesh refinement and adaptive higher order discretization codes. Existing codes of the Center partners and new codes are supported to create a plug and play capability, whereby an application user can experiment easily with alternative technologies. Insertion of these tools into targeted applications is part of the Center work plan.

CSC work within TSTT currently focuses on jet breakup, spray formation, and on finite element and front tracking contributions to TSTT technology.

4.1.2 TOPS

D. Keyes

Terascale Optimal PDE Simulations (TOPS) is a second SciDAC project connected to Brookhaven. TOPS software is being applied in CSC through a collaboration with one of its principal investigators. TOPS deploys a toolkit of open source solvers for partial differential equations, large systems of stiff ordinary differential equations, and linear and nonlinear algebraic systems, including eigenvalue problems, that arise application areas such as accelerator design, biology, chemistry, magnetohydrodynamics, and particle physics. Scalable solution algorithms -- primarily multilevel methods -- aim to reduce computational bottlenecks by one or more orders of magnitude on terascale computers, enabling scientific simulation on a scale heretofore impossible. Along with usability, robustness, and algorithmic efficiency, an important goal is to attain high computational performance by accommodating to distributed hierarchical memory architectures.

The convergence rates of solvers traditionally employed in PDE-based codes degrade as the size of the system increases. This creates a double jeopardy for applications -- as the cost per iteration grows, so does the number of iterations. Fortunately, the physical structure of PDE problems, such as Poisson's equation for electrostatic potential, provides a natural way to generate a hierarchy of approximate models, through which the required solution may be obtained efficiently. The philosophy that underlies optimality is to make the majority of progress towards a high fidelity result through inexpensive intermediate stages.

The efforts defined for TOPS and its collaborations incorporate existing and new optimal algorithms into scientific applications through code interoperability behind a standard interface. TOPS provides support for the software packages Hypre, PARPACK, PETSc (which has powered two Gordon Bell Prizes in recent years), ScaLAPACK, Sundials, SuperLU, and TAO. Some of these packages are in the hands of thousands of users, who have created a valuable experience base on thousands of different computer systems.

The TOPS project webpage may be found at http://www.tops-scidac.org .

4.1.3 Advanced Computing for 21st Century Accelerator Science and Technology

R. Samulyak

The SciDAC Accelerator Modeling Project, "Advanced Computing for 21st Century Accelerator Science and Technology," was initiated in June 2001. Its primary goal is to establish a comprehensive terascale simulation environment for use by the U.S. particle accelerator community. Building upon a previous DOE Grand Challenge project as well as previous individual efforts at several national laboratories and universities, the SciDAC Accelerator Modeling Project represents the largest effort to date for the development of computer codes for accelerator design and analysis. The activities of the project are organized into three application-specific focus areas: Electromagnetics, Beam Dynamics, and Advanced Accelerators. Work in these areas is supported by collaboration with the SciDAC Integrated Software Infrastructure Centers (ISICs) and by personnel (including CSC/BNL) supported through the SciDAC Scientific Application Partnership Program (SAPP).

Research at CSC/BNL is conducted in close collaboration with the Beam Dynamics group. The primary goal of the study is the development of novel mathematical models and software modules for the computation of wake fields and their interaction with particle beams in high intensity accelerators. We have implemented our software in the MaryLie/Integrated Map and Particle Accelerator Tracking code, a parallel code that combines the magnetic optics capabilities based on the Lie algebraic technique with the 3D space charge capabilities. Currently we have been working on the implementation of the wakefield module in the Synergia framework. We have also joined the LBL/LANL effort to develop methods and high performance software tools for modeling the electron cooling and intrabeam scattering. These processes present the most important obstacles for the future upgrade of high-energy accelerators such as RHIC at BNL and Tevatron at FNAL. To provide tools for numerical studies of the electron cooling and intrabeam scattering, a code for solving the Fokker-Plank equation will be developed based on the self-consistent Langevin approach, with the diffusion and damping coefficients computed from first principles based on the Rosenbluth potentials. The problem presents significant computational challenges even for modern supercomputers.

4.2 BIOLOGICAL AND ENVIRONMENTAL RESEARCH

Novel algorithms and hardware allow fine-scaled parallelism for all atom simulations to model structural biology. We project long simulated times (1-10 μsec for all atom simulations). This

result will allow exploration of new time scales in structural biology. We are emphasizing conformational changes in proteins with known structures, in collaboration with BNL biologists.

Brookhaven has strong experimental programs in atmospheric chemistry and brain physiology. Both programs are data intensive. The challenge is not only data quantity, but especially data understanding. We have developed new tools for interactive visual and statistical data analysis. We are actively using these tools in diverse applications. See also Section 4.3.4.

4.2.1 MD Simulations of the Activation of the Adenovirus Proteinase

J. V. Stern, W. J. McGrath, J. W. Davenport, and W.F. Mangel

The adenovirus proteinase (AVP) is a relatively inactive enzyme that can be activated by an 11-amino-acid peptide cofactor, pVIc [1,2]. The binding of pVIc increases the activity of AVP more than 3500-fold. The crystal structure of the AVP-pVIc complex has been determined experimentally using x-ray diffraction and the pVIc peptide was found to bind to AVP in an extended conformation quite far from the active site, as shown in Figure 1 [3]. The peptide traverses the surface of the protein, ranging from 14 Å to more than 30 Å away from the active site. This raises the question: How can the binding of pVIc quite far from the active site have such a profound influence in the functioning of the enzyme? Very recently, the crystal structure of AVP in the absence of the cofactor was solved as well. Comparison of this structure to the structure of the AVP-pVIc complex is revealing how pVIc activates the enzyme. We hypothesize that in order for the binding of pVIc to activate the enzyme, a signal must be transduced by a sequence of structural changes beginning at the pVIc binding site on AVP and ending in the active site of AVP. Using molecular dynamics simulations it is hoped that the sequence of structural changes which occurs can be understood and exploited to provide targets for drugs. If the binding of a drug to a target within the sequence of structural changes can prevent the signal from being transduced, therefore preventing activation, the drug could be an effective anti-viral agent.

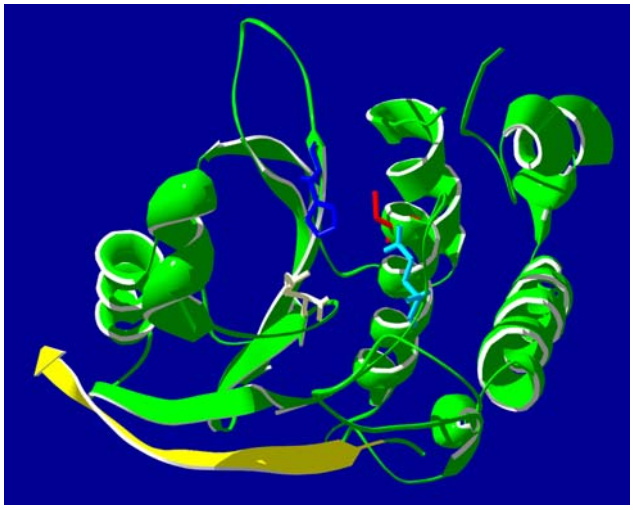

Figure 1. Crystal structure of AVP-pVIc. The four amino acids involved in catalysis are Cysteine122 (red), Histidine54 (blue), Glutamic acid71 (white) and Glutamine115 (turquoise); they are located in the active site, a long groove. The β-strand of pVIc is in yellow.

The molecular dynamics (MD) simulations are being performed using NAMD [4] a parallel molecular dynamics code designed for high-performance simulation of large biomolecular systems. We use the AMBER force fields [5] and carry out standard MD simulations at constant temperature and pressure with explicit TIP3P waters added [6]. Our protein contains 204 amino acids plus the 11 amino acid peptide cofactor. After protonation this constitutes about 3500 atoms. Adding water yields a total of 30,000 atoms. Using this approach, one possible step in the activation mechanism has been observed, the final step in pVIc binding to AVP illustrated in Figure 2.

We have a model of how pVIc binds to AVP, deduced from inspection of the crystal structures of the two end states, and we have asked the question: Can molecular dynamics simulations be used to see the reverse reaction, i.e. the unbinding of pVIc from AVP-pVIc? We hypothesize that the two N-terminal amino acids of pVIc bind to a surface pocket in AVP. Then, the remaining amino acids of pVIc bind in sequence, one at a time, to AVP. Upon the binding of the last three amino acids of pVIc, a surface pocket is induced in AVP to envelop the last three amino acids. The last amino acid residue in pVIc, a phenylalanine, caps the newly formed pocket. Then, the penultimate amino acid in pVIc, a cysteine residue, forms a disulfide bond (covalent bond) with AVP.

Starting with the AVP-pVIc structure but one in which the cysteine residue of pVIc has been mutated to an alanine, thereby removing the disulfide bond, can we see the reverse of the peptide binding sequence, i.e. the leaving of the last three amino acids of pVIc from the induced pocket?

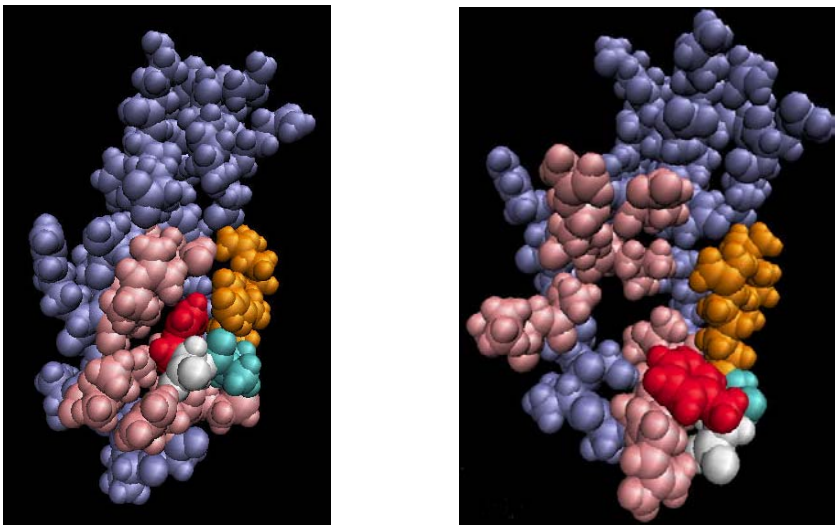

Figure 2. Van der Waals representation of a mutant of AVP-pVIc at 2.5ps (left) and 102.5 ps (right). Color Scheme: pink – pocket; red – PHE ring (the ring that caps the pocket); white – PHE tail; cyan and orange – adjacent pVIc amino acid residues; blue – adjacent AVP amino acid residues.

Indeed, molecular dynamics simulations show the last three amino acids of pVIc leaving the induced pocket, Figure 2. By 102.5 ps, the PHE ring (red) and its tail (white) have left, and the compositon of the surface where the last three residues of pVIc were located has changed. We plan to continue these simulations to elucidate the transformations involved in activating the enzyme

and to discover sites along the pathway that may serve as targets for drugs that will act as antiviral agents.

References

[1] Mangel, W.F., McGrath, W.J. et al.. Viral DNA and a viral peptide can act as cofactors of adenovirus virion proteinase activity. Nature **361**: 274-275 (1993).

[2] Mangel, W.F., Baniecki, M.L., and McGrath, W. J. Specific interactions of the adenovirus proteinase with the viral DNA, an 11-amino-acid viral peptide, and the cellular protein actin, CMLS, Cell. Mol. Life Sci. **60:** 2347-2355 (2003).

[3] Ding, J., McGrath, W.J., et al.. Crystal structure of the human adenovirus proteinase with its 11 amino-acid cofactor. EMBO J. **15**: 1778-1783 (1996).

[4] Laxmikant, K.R., et al. NAMD2: Greater scalability for parallel molecular dynamics. Journal of Computational Physics **151**: 283-312 (1999).

[5] Cornell, W.D., Cieplak, P. et al. A second generation force field for the simulation of proteins, nucleic acids, and organic molecules. J. Am. Chem. Soc. **117**: 5179-5197 (1995).

[6] Jorgensen, W.L., Chandrasekhar, J. et. al.. Comparison of simple potential functions for simulating liquid water. J. Chem. Phys. **79**: 926-935 (1983).

4.2.2 Structural Analysis of Botulinum Neurotoxin

Y. Deng, X. Chen, Y. Chen, B. Fang, G. Han, and P. Rissland

The toxin produced by the bacterium Clostridium botulinum is one of the deadliest known [1]. Recently a great deal of information about its mode of action has become available through structural and other biophysical studies. The toxin itself (BoNT) is a protein of approximately 1300 residues. It is made up of two chains, a light chain (LC) of approximately 50 kDa and a heavy chain (HC) of approximately 100 kDa. The two are linked by a disulfide bond. The light chain contains a Zn^{2+} ion which acts within the cell to cleave a protein necessary for neurotransmission leading to paralysis and death. This process is believed to involve several steps: binding of the toxin to the endosomal membrane, translocation through the lipid bilayer, and proteolysis of specific neurotransmitters within the cell. The structural studies show that the heavy chain contains two domains responsible for binding and translocation while the light chain contains the catalytic domain. Both the structure of the toxin outside the cell (but not at endosomal pH) and the mechanism of action of the zinc protease are reasonably well understood. What is not known are the structures at low pH (5.1-5.4) and the mechanism of translocation.

We have begun to study these two aspects in detail using highly parallel molecular dynamics and energy minimization codes. The force filed used is:

$$E = \sum_{bonds} \frac{a_i}{2}(l_i - l_{i0})^2 + \sum_{angles} \frac{b_i}{2}(\theta_i - \theta_{i0})^2 + \sum_{torsions} \frac{V_n}{2}(1 + \cos(n\omega - \gamma))$$
$$+ \frac{1}{2}\sum_{i=1}^{N}\sum_{j\neq i}^{N} 4\varepsilon_{ij}\left[\left(\frac{\sigma_{ij}}{r_{ij}}\right)^{12} - \left(\frac{\sigma_{ij}}{r_{ij}}\right)^{6}\right] + \frac{1}{2}\sum_{i=1}^{N}\sum_{j\neq i}^{N}\frac{q_i q_j}{r_{ij}}$$

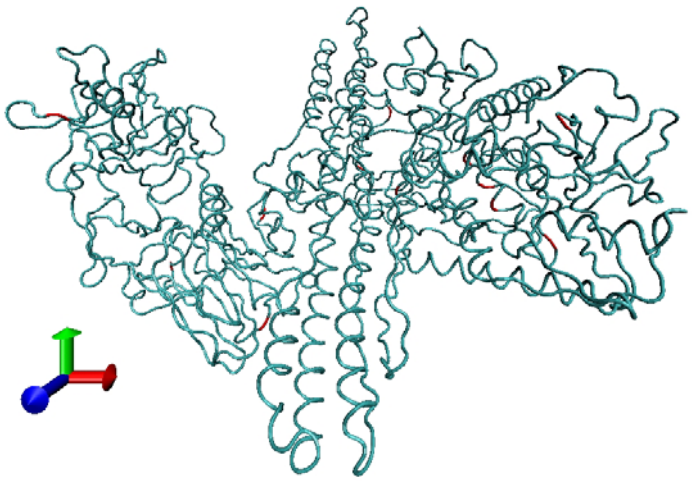

Figure 3. Botulinum with residuals marked red for alteration for constant pH modeling.

We have developed a parallel molecular dynamics code MDoC (Molecular Dynamics on a Chip), a package designed by our group for ultrascalable architectures, such as IBM's BG/L and Columbia's QCDOC. It uses the PDB and Amber [2] parameter files that are commonly employed in popular MD simulation packages. These files are generated to describe the molecular systems to be simulated, such as atom positions, force constants, charges, mass, etc. This enables the direct use of pre-existing files in MDoC without additional effort. MDoC uses Ewald summation to compute the Coulomb forces with complexity $O(N^{3/2})$ for N particles. Our MDoC for ultrascalable architectures is designed to exploit the multiple dimensional tori network topologies by tailoring MPI functions to achieve the optimal network load balance and maximal wire utilization during the electrostatic force calculation for which positions and charges of all particles must be passed to all processors. The core of MDoC centers on exploiting the new torus networks in the ultrascalable architecture that was not incorporated in any earlier MD packages. The code also integrates new algorithms for FFT and multiple time stepping.

It is well known that the structure and function of proteins are strongly pH dependent. This dependence is due to changes in the predominant protonation state of titratable groups as solvent pH changes. The protonation state of a titratable group is also determined by its pKa. On the other hand, pKa of a given group is influenced by the protein conformation. Therefore there is a tight coupling between protein conformation and protonation state. However, the traditional treatment of pH in MD has been limited to setting a constant protonation state for each titratable group. This approach decouples this dynamic dependence. Recently a new approach combining MD and

Monte Carlo simulation has been developed. We plan to use this new method to validate our current results and to implement it into our own code.

References

[1] Turton, K., Chaddock, J. A., and Acharya, K. R. Botulinum and tetanus neurotoxins: structure, function and therapeutic utility. Trends in Biochemical Sciences **27:** 552-558 (2002).

[2] AMBER: http://www.amber.scripps.edu

4.2.3 Molecular Dynamics on the QCDOC

J. Davenport, Y. Deng, and J. Glimm

Molecular dynamics simulations [1, 2] are ideal for massively parallel computing because the time spent on communication can be a small fraction of the time spent on computation. However, most molecular dynamics (MD) simulations have been performed on machines where this potential has not been realized due to slow communication limiting the effective use of large numbers of processors.

We have explored [3] the use of a new machine designed for quantum chromodynamics (QCD) by a team of elementary particle physicists [4] mainly at Columbia University, The Riken BNL Research Center and IBM. This machine consists of approximately 10,000 IBM PowerPC processors with extremely fast nearest neighbor communication and 4 megabytes of memory located on each chip. For this reason, it has been named QCDOC for quantum chromodynamics on a chip. It is expected to achieve of order 5 teraflops (or 5×10^{12} floating point operations per second) at a cost of roughly $500 per processor.

We project a dramatic level of fine scale parallelism for molecular dynamics simulations based on novel architectural and algorithmic principles, for this machine and its successor, Blue Gene / Light.

The architectural principle is the 6D mesh communication topology, supported by 24 wires per processor (bidirectional send/receive for each mesh dimension). This mesh can be thought of as a programmable distributed switch, and at the level of 10K processors or more, it vastly outperforms technologically feasible switches in terms of effective bandwidth and latency, as well as cost.

The algorithmic principle is fine-scaled parallelism enabled by the rapid communication, i.e. small problem sizes per processor. We plan to compute entirely within L2 cache, and completely avoid the bottleneck of communication delays to main memory. With fine-scaled parallelism, we assign about 10 particles per processor.

We project an ability to simulate 1-10 μsec of real time for all atom MD simulations of 10K to 100K atoms using this machine. We have developed algorithmic and hardware performance models to support this prediction.

References

[1] Allen, M.P. and Tildesley, D.J. *Computer Simulation of Liquid.* Oxford, New York, 1987.

[2] Frenkel. D. and Smit, B. *Understanding Molecular Simulation*. Academic, San Diego, 1996.

[3] Deng, Y., Glimm, J., Davenport, J., Cai, X., and Santos, E. Performance models on QCDOC for molecular dynamics with Coulomb potentials. Int. J. High Performance Computing Applications **18(2)**: 183-198 (2004).

[4] Chen, D., Christ, N.H., Cristian, C., Dong, Z., Gara, A., Garg, K., Joo, B., Kim, C., Levkova, L., Liao, X., Mawhinney, R.D., Ohta, S., and Wettig, T., hep-lat/0011004.

4.2.4 Detection of Cancer

W. Zhu and J. Kovach

At an early stage, ovarian cancer has a high (90%) cure rate, but cannot be readily detected. At late stages, when detection usually occurs, the cure rate is 35%. Annually, 14,500 women die from this disease in the U.S. Mass spectrum analysis of protein fragments in blood samples has been proposed by Petricoin et al. (reported in Lancet [1]) as a diagnostic tool, specifically for diagnosis of cancer. The idea has two steps. The hardware, or physical measurement step, is by a mass spectrometer. This machine looks at blood fractions and trace proteins, and records mass (in relation to charge). Of course there are many hundreds of thousands of these signals ("markers"). The second step is to find the needle in the haystack. Which markers distinguish a normal patient from one with ovarian cancer? This is a problem in statistics and its solution enables the diagnostic procedure. Professor Wei Zhu, CSC staff member and member of the Department of Applied Mathematics and Statistics, John Kovach, MD, Director of the Long Island Cancer Center and a team of graduate students have made significant process with the pattern recognition problem [2].

The statistical problem is solved using diagnostic data, that is, blood samples from patients with known diagnosis, having ovarian cancer or normal. The data is divided in half, one half to train the statistics and the other half to test the conclusions. All markers are assessed for their ability to distinguish between normal and afflicted patients in the training set. About 150 markers show a statistically unusual pattern of difference between these populations. This number depends on the resolution power of the mass spectrum equipment. A subject with a positive reading on selected markers is predicted as possibly afflicted with ovarian cancer. When the test is applied to the testing set, accuracy in the range of 80-95% results.

[1] Petricoin III, E.F., Ardekani, A.M., Hitt, B.A., Levine, P.J., Rusaro, V.A., Steinberg, S.M, Mills, G.B., Simone, C., Fishman, D.A., Kohn, E.C., and Liotta, L.A. Lancet **359:** 572-577 (2000) and Lancet **360:** 169-171 (2002).

[2] Zhu, W., Wang, X., Ma, Y., Rao, M., Glimm, J., and Kovach, J. Detection of cancer specific markers amidst massive mass spectral data. Proc. Nat. Acad. Sci. **100:** 14666-14671 (2003).

4.2.5 Cardiac Electrophysiology

S. Evans, F. Fenton, J. Glimm, H. Hastings, and W. Oh

Sudden cardiac failure is a major cause of death. The causes and conditions leading to sudden cardiac death are complex and varied, and have been the subject of extensive studies. In collaboration with researchers from Hofstra University and Beth Israel Medical Center, we have been studying the dynamics of ventricular fibrillation, an irregular and chaotic heart rhythm that almost always results in sudden cardiac death.

We model cardiac electrophysiology through computer simulation. For this purpose it is common to use the monodomain equation that limits the electrical activity within cells. In reality, the ion-mediated current travels into and out of cells, requiring a bidomain model to more accurately simulate complex cardiac electrophysiology, using the equations

$$\begin{aligned} \frac{\partial_u}{\partial_t} &= \frac{1}{\chi C_m}\nabla\cdot\sigma_e\nabla u_e + \frac{f(u)}{R_m C_m}, \\ \nabla\cdot\sigma_i\nabla u + \nabla\cdot\left(\sigma_i+\sigma_e\right)\nabla u_e &= 0. \end{aligned} \tag{1}$$

Here u_i and u_e are the intra and extra cellular potentials, $u = u_i - u_e$ is the transmembrane potential, F_i and F_e are conductivity tensors, and C_m, R_m, and χ are the membrane capacitance, membrane resistance and surface-to-volume ratio. The reaction term f(u) represents the ionic current.

We developed a parallel code to solve the bidomain equations in 2d and 3d. With this code, we will be able to study the onset and the dynamics of ventricular fibrillation.

In Figure 4, we present a 3D simulation using the bidomain code. The transmembrane potential is plotted at 100 msec intervals. An initial stimulus at the center of the domain has propagated radially. The first frame is at 100 msec. Since we used anisotropic conductance, the wave propagates with slightly different speeds in the x. y and z directions. At t=215 msec (before the third frame), we stimulated the center again and observed scroll waves. One practical way to identify the scroll wave is to arbitrarily choose a single isopotential surface of constant potential u(x,t)=c. The wave tip, or vortex filament, can be defined as the intersection of u(x,t)=c and \partial_t u = 0. In Figure 5, we present the dynamics of the vortex filament starting at 300 msec at 100 msec interval.

The simulations will be validated by comparison with experimental data, and the code will be used in a large-scale study of wave stability and scroll wave dynamics in realistic 3D anatomy. Large-scale simulations will provide critical insights into basic cardiac physics and dynamics. Moreover, the use of these models will allow experiments that cannot be performed with animal models because variability among individuals within a species makes it difficult to isolate causal factors.

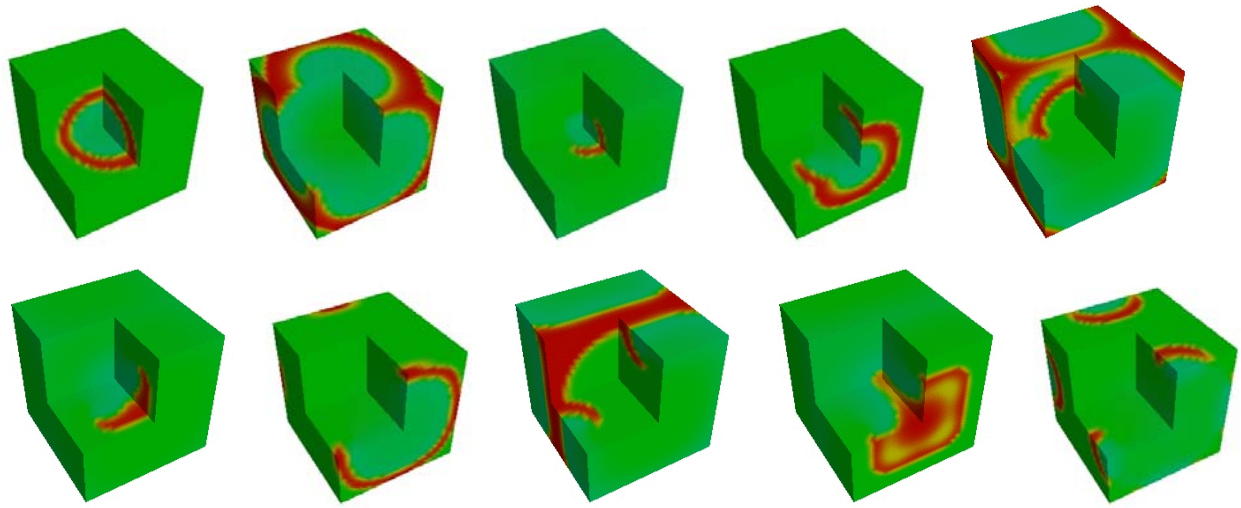

Figure 4. Successive time frames showing the propagation of the transmembrane potential and development of scroll waves, based on the bidomain equation.

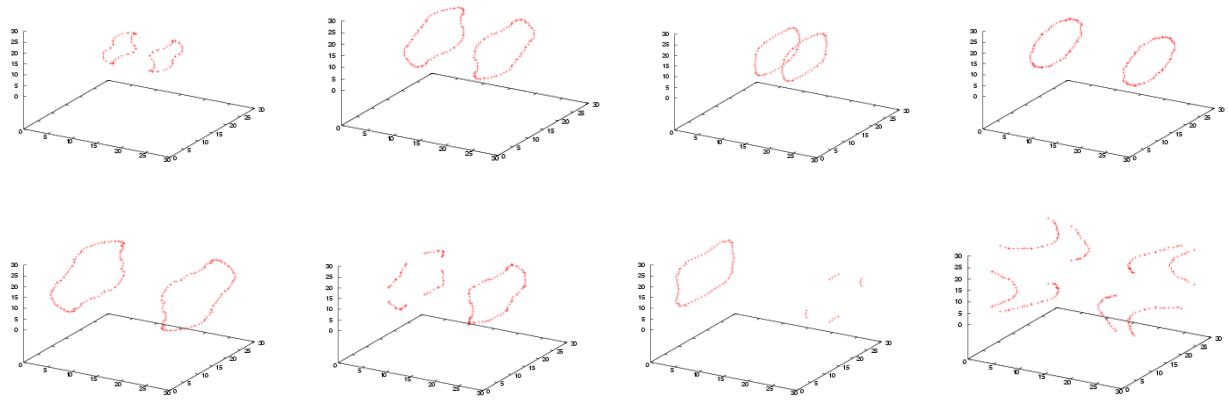

Figure 5. Successive time frames showing the vortex filament of the scroll waves shown in Figure 4.

References

[1] Fenton, F. and Karma, A. Vortex dynamics in 3D continuous myocardium with fiber rotation: fibrillation. CHAOS **8:** 20 (1998).

[2] Fenton, F., Evans, S., and Hastings, H.M. Memory in an excitable medium: A mechanism for spiral wave breakup in the low excitability limit. Phys. Rev. Lett. **83:** 3964-3967 (1999).

[3] Hastings, H.M., Fenton, F., Evans, S., Hotomaroglu, O., Geetha, J., Gittelson, K., Nilson, J., and Garfinkel, A. Alternans and the onset of ventricular fibrillation. Phys Rev E **62:** 4043-4048 (2000).

[4] Keener, J.P. and Bogar, K. A Numerical method for the solution of the bidomain equations in cardiac tissue. Chaos **8(1):** 234-241 (1998).

[5] Fenton, F.H., Cherry, E.M., Hastings, H.M, and Evans, S.J. Multiple mechanisms of spiral wave breakup in a model of cardiac electrical activity. CHAOS **12 (3):** 852-892 (2002).

4.2.6 Atmospheric Aerosols

W. Zhu, K. Mueller, and S. Schwartz

The purpose of this project is to develop data processing tools for the classification and time series analysis of atmospheric aerosol particles. Atmospheric aerosols play an important role in both climate and public health. Current research is focused on determining the chemical composition of aerosols, and thus the composition of air and its evolution over time. Massive mass spectra data, on the scale of terabytes per week, have been collected continuously over time by researchers in the Atmospheric Sciences Division at Brookhaven, using their cutting-edge, field deployable high precision mass spectrometer. The first task is to determine the chemical composition of each aerosol based on its mass spectrum. To achieve this, we classify aerosols by their chemical compositions and thus determine the air composition at each time point. Finally, we study the time series evolution of atmospheric compositions identifying normal as well as abnormal patterns in real time.

To convey the analysis results to the scientists in an intuitive way and to incorporate their expert knowledge into the data analysis phase, an interactive graphical user interface utilizing modern scientific visualization techniques becomes a necessity. Large-scale BNL data collections have reached sizes for which straightforward visualization techniques are starting to fail. In this spirit, our proposed approach couples a powerful Bayesian classification and multivariate time series analysis engine with an intuitive and responsive graphical user interface to fine-tune the underlying models. We call this application *SpectrumMiner*, a significant component of a more general visual data mining framework and application, called ViStA, which we are currently developing at BNL (for more detail see Section 4.3.4).

The statistics engine. We first classify aerosols based on their mass spectra through an iteration of expert-machine interaction using a Bayesian classifier. The Bayesian classifier can incorporate not only explicit classification rules but also prior knowledge in terms of a partial training data set. We have also been implementing automatic procedures to elucidate the structure of the compounds. To study the evolution of aerosols and the changes in atmospheric composition versus time, both the univariate and the multivariate time series analyses are employed to unravel trends and patterns.

The traditional statistical classifier would take only explicit classification rules. Machine learning techniques such as the neural network would take only a training set. However, the semi-supervised clustering approach we are taking requires the classifier to learn from both the explicit rules and the implicit rules embedded in a partial training set established by the experts as they survey the current clustering results and make adjustments to the clusters. For this we have implemented an interactive Bayesian classification framework that could absorb the up-to-date

prior information in both the explicit and implicit formats, and produce the updated posterior classification results.

For efficient classification and automatic structure elucidation, we have been constructing a molecule library where the signature profile and class membership of each molecule is established. The molecules are classified along a natural chemical classification tree with two categories--organic and inorganic--at the initial node. Subsequently, the organics are further divided into classes of carboxylic acids, aldehydes, ketones, alkenes, alkanes, aromatics, etc. We begin with the spectra of known molecules (NIST library or lab-generated).

Visualization. The statistical analysis engine is combined with a highly visual interface to facilitate interactive exploration, mining, classification and survey of these large, high-dimensional data collections. In order to empower scientists to control and fine-tune the mining and classification process in an intuitive and interactive way, SpectrumMiner's hierarchical classification algorithm is user-steerable via a novel multi-modal visual interface. An important component of this interface is the *interactive dendrogram* [1], where hierarchy nodes are placed on concentric circles whose radii are determined by the dissimilarity of the node's sub-tree. We chose a circular layout of the dendrogram since it makes better use of space than its linear counterpart. It inherently dedicates less drawing space to the higher-level, less numerous nodes, and distributes more space to the many leaf nodes along the circumference of the circle. See Figure 6, where we show a screen capture of SpectrumMiner, with the interactive dendrogram located on the bottom right. Edges are colored using a rainbow colormap to indicate the number of data items they carry. To the left of the dendrogram is the node viewer. Selecting a particular node will display the average spectrum of all data items classified into the node (window with white background), as well as the node's data composition (window with blue background just below). We are currently incorporating the classification steering capabilities into our system. By inspecting the present classification in the node viewer and the dendrogram, scientists may decide that some particles, or the entire node, have been misclassified. To correct this error, they then simply drag the concerned particles or node into the proper location within the hierarchy, which subsequently triggers a refinement of the classification rules.

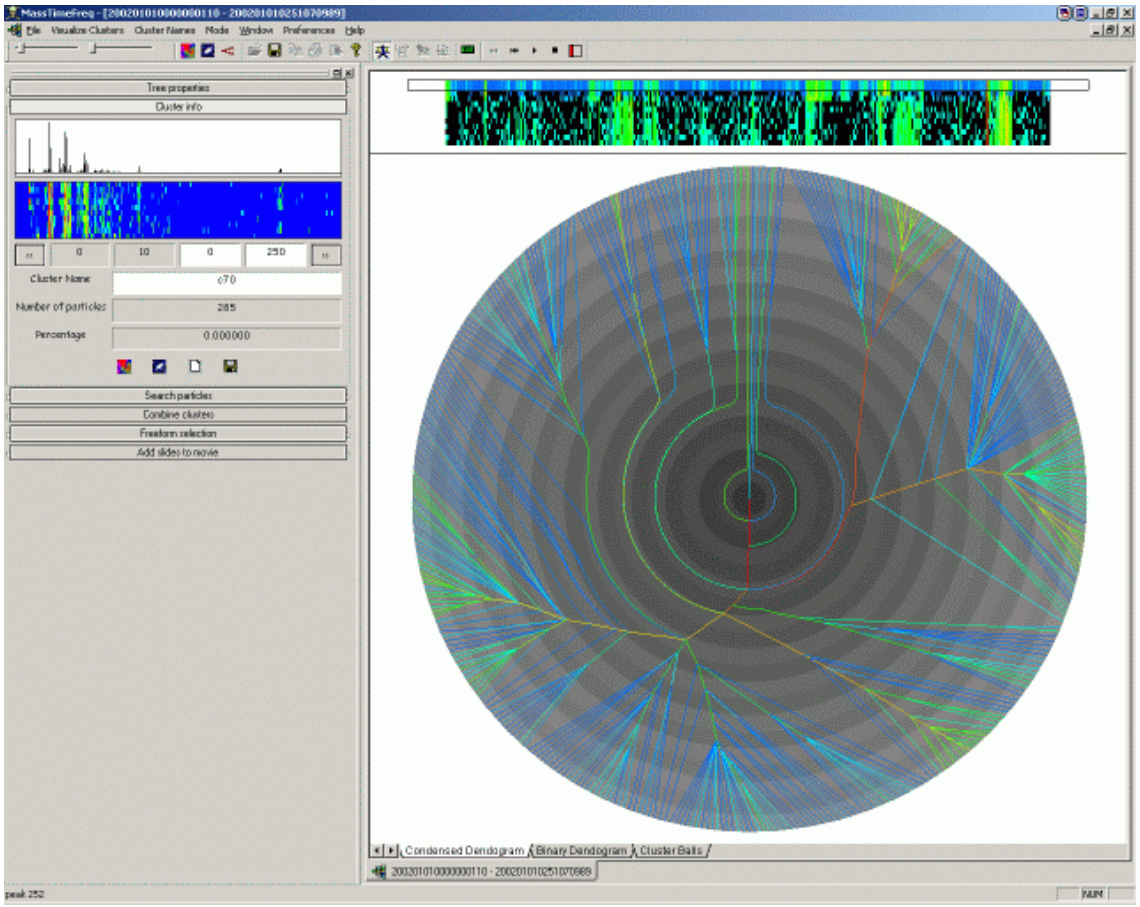

Figure 6. SpectrumMiner's interactive dendrogram interface.

Reference

[1] Imrich, P., Mugno, R., Mueller, K., Imre, D., Zelenyuk, A., and Zhu, W. Interactive poster: Visual data mining with the interactive dendrogram. Information Visualization Symposium, 2002.

4.2.7 Interactive Visualization of Modeled Atmospheric Trace Constituents

C. M. Benkovitz, R. E. Bennett, and L. A. Slatest

The purpose of this project is the development of 3-dimensional visualization techniques for the Brookhaven National Laboratory Chemical Transport Model (CTM) of atmospheric sulfate. The techniques described here can be applied to any atmospheric trace constituents – aerosols (such as dust or anthrax spores), gases (such as sulfur dioxide or sarin) and liquids (such as cloud droplets).

Aerosols are microscopic particles suspended in the atmosphere which can be liquid or solid. Aerosols can influence climate, depending on their size and composition. Aerosol diameters (in μm, 10^{-6} m) relevant to climate include: a) nuclei mode: 0.005 to 0.1, b) accumulation mode: 0.1 to 2.5 (these particles become cloud condensation nuclei, CCN), and c) coarse: > 2.5. In contrast, the diameter of cloud droplets (CD) is > 10 μm. The climate influences of tropospheric aerosols are

exerted in two ways: a) Direct Radiative Forcing: scattering and absorption of shortwave radiation by aerosols, and b) Indirect Radiative Forcing: changes in cloud microphysical properties influencing the irradiative properties. Both these influences have a cooling effect on climate.

Anthropogenic activities have a strong effect on the aerosol content of the atmosphere. Emissions increase CCN, which increases CD, which increases cloud albedo, which leads to a cooling effect on climate. Aerosols can be emitted directly as particles, for example from industrial activities, biomass burning, mineral dust sources (deserts, tilled fields, etc.), sea salt or as gaseous sulfur precursors which are converted to sulfate particles in the atmosphere, for example SO_2 from industrial activities, dimethyl sulfide (DMS) from biogenic ocean and land processes, SO_2 from volcanoes (degassing and erupting), SO_2 from biomass burning.

Studies of the influence of aerosols on climate are hindered by the sparcity of observations of the mixing ratios in time and space. Therefore, regional to global chemical transport models are needed. The amount of data resulting from such simulations is very large, requiring new techniques.

Figure 7 presents a schematic of the components of the BNL CTM for sulfate. The results to be presented were taken from a simulation of the Aerosol Characterization Experiment (ACE-2) with the following characteristics: domain included the Northern Hemisphere to 81N, 360 × 81 × 27 grid cells (787,320), 25 species: 6 SO_2 (by source region), 16 sulfate (by source region & conversion pathway), MSA, DMS, H_2O_2. Time period: simulation from June 1 to July 25, 1997, analyses start June 17, 1997.

Figure 8 presents a 3-dimensional display of the model-calculated sulfate mixing ratios (MRs, parts sulfur/part air) for June 22, 1997. The figure is a volume rendering; blue -> red is lower -> higher MRs. The rectangle over western Mexico shows the effects of the emissions of Popocatepetl volcano, located near Mexico City. The effects of stronger emissions in Europe and Asia are prominent on this date.

Future work will improve the rendering. For example, our vertical grid is unevenly spaced whereas here it is represented as evenly spaced, values of the MRs span several orders of magnitude so in place of the adjusted linear scale used here a logarithmic scale would allow greater range of display.

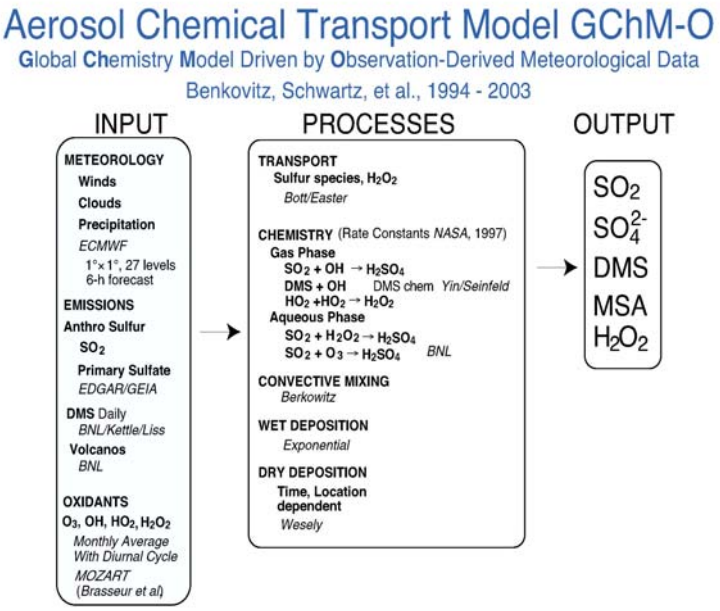

Figure 7. Schematic aerosol transport model.

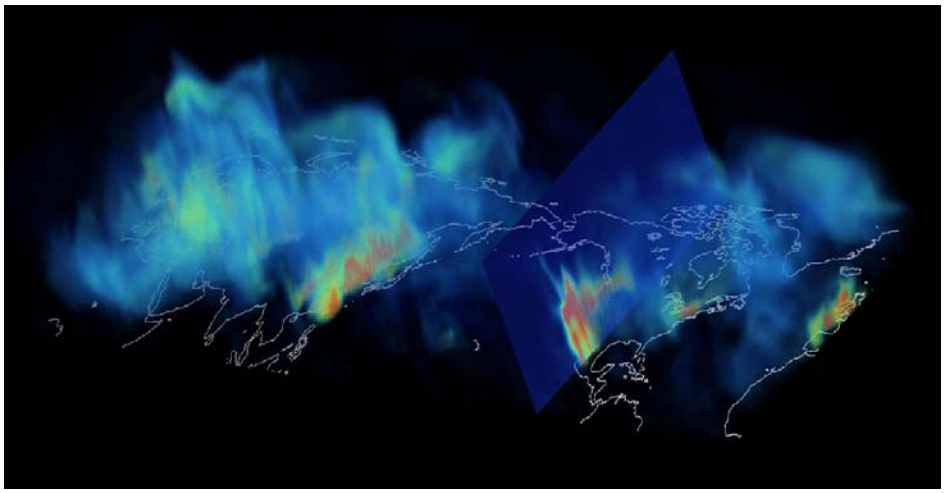

Figure 8. Vertical aerosol distribution shown on a series of planes.

References

[1] Benkovitz, C.M., Schwartz, S.E., Jensen, M.P., Miller, M.A., Easter, R.C., and Bates, T.S. Modeling atmospheric sulfur over the Northern Hemisphere during the ACE-2 experimental period. J. Geophys. Res., in press (2004).

[2] Benkovitz, C.M., Schwartz, S.E., and Kim B.-G. Evaluation of a chemical transport model for sulfate using ACE-2 observations and attribution of sulfate mixing ratios to source regions and formation processes. Geophys. Res. Lett. **30:** 1641 (2003).

4.3 ADVANCED SCIENTIFIC COMPUTING

4.3.1 TSTT: Atomization and Spray

J. Glimm, M.N. Kim, X. Li, A. Marchese, R. Samulyak, C. Tzanos, and Z. Xu

TSTT: Jet Breakup and Spray Formation in a Diesel Engine

In the past year, we have studied the mechanisms leading to jet breakup and spray formation for a high speed diesel jet injected through a circular nozzle. We have used the Front Tracking method [1]. Many parameters such as the nozzle shape, the velocity and the turbulence of the jet, and the thermodynamic states of liquid and gas are believed to be contributing causes to the breakup. We conduct the simulations for the jet breakup within a 2D axis-symmetric geometry. Our goal is to model the spray at a microphysical level, with the creation of individual droplets. We have used a heterogeneous EOS model consisting of explicitly tracked vapor bubbles within the liquid diesel fuel for the mixed phase (diesel vapor/liquid) regime. For comparison, we also study the simulations based on the homogeneous description of the mixed phase region in the jet flow.

Through our study, we have found that the flow in the jet leaving the nozzle is too fast and the breakup is too rapid for Kelvin-Helmholtz instabilities to be the primary driving force for the breakup at the jet surface. We conclude that there are other significant events in the nozzle flow upstream of the jet to provide the breakup mechanism. The flow is at high Reynolds number, but due to the short length of the nozzle, we find that the pure liquid flow is laminar, i.e. non-turbulent, under experimental conditions.

We have observed the formation of vapor cavitation in the flow, which indicates the vaporization of the liquid. We now use the finite sized saturated vapor bubbles to represent this mixed liquid-vapor region. We have implemented the dynamic creation of vapor bubbles. The size of the bubbles and the spacing between bubbles during the initialization are adjustable parameters, and are determined by numerics. The vapor is modeled by a gamma law gas. The interface which separates the liquid and the vapor is modeled as a phase boundary.

The phase transition is governed by the compressible Euler equations with heat diffusion. We have developed numerical algorithms for the solutions of dynamical phase transitions. The bubbles grow or shrink due to the thermal effects of evaporation and condensation, but especially due to the passage of transient pressure waves up and down the nozzle. We allow continuous temperature and a pressure jump at the phase boundary. The phase boundary is solved by using thermal and phase boundary equations. This is a new description for the Riemann problem associated with a phase transition in a fully compressible fluid.

We also implemented a homogenized EOS with a mixed liquid-vapor region to model fine scale bubbles and droplets (see Section 4.4.4). The sound speed in the mixed phase region is very small, and so the flow in the mixed phase region is highly supersonic. It turns out that highly supersonic flow strongly suppresses vorticity, so that with this EOS model, the nozzle flow is still laminar. Thus the EOS with a homogenized mixed phase region does not produce jet breakup.

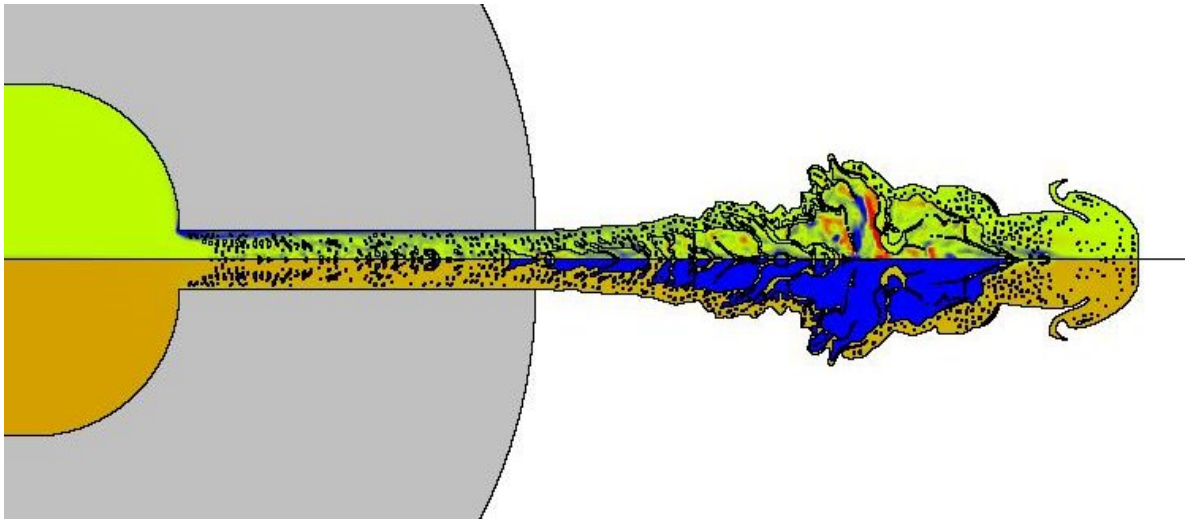

Figure 9. The vorticity (above) vs. density (below). The dark spots are the diesel vapor bubbles. The bubbles appear and disappear as rarefaction waves progress up and down the nozzle. The large blue region in the lower frame is a vapor region.

We have compared our simulation with the experimental data [2, 3, 4, 5]. We measured the mass in a 0.55mm wide observation window which is centered 1mm downstream from the nozzle exit. The mass from our calculation displays a transient peak which is 20~35% higher than the experimental data. We also measured the jet tip velocity. It is 40~50% slower than that from the experiment.

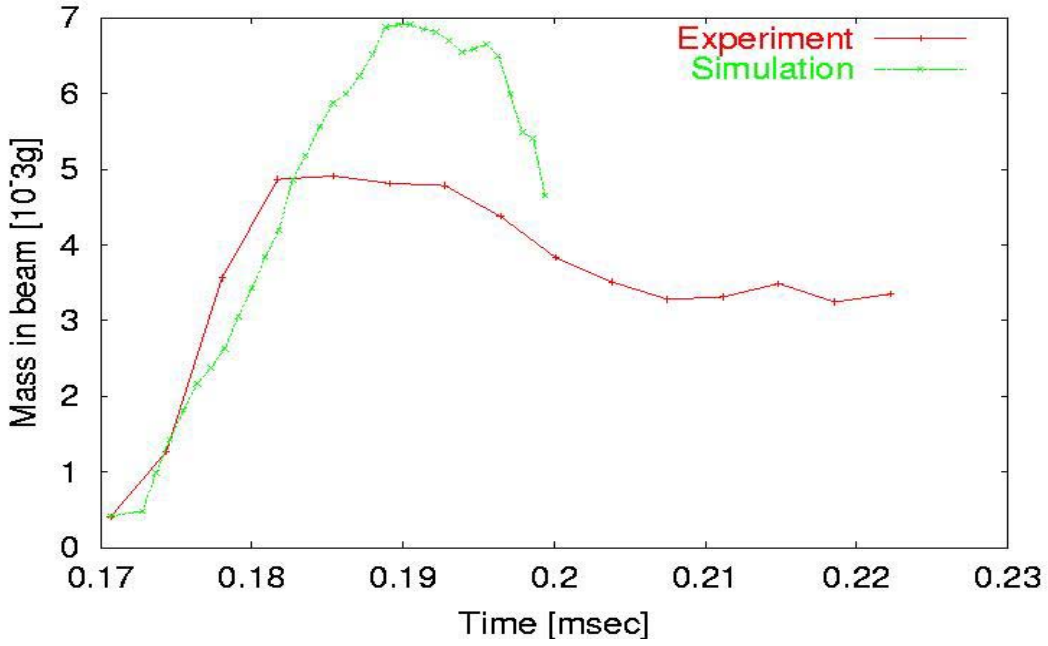

Figure 10. The plot of mass at 1mm from the nozzle exit.

The finite sized vapor bubbles improve the mass in the experimental region. It slows down the jet tip velocity relative to experimental measurements in comparison to the homogeneous EOS model of the mixed phase region. We are conducting the mesh refinement studies by using the adaptive

mesh refinement in the front tracking method [6,7]. The influences of the other parameters on the spray formation will be the object of further study.

References

[1] Glimm, J., Oh, W., Marchese, A., Li, X, Xu, X., Kim, M.-N., Samulyak, R., and Tzanos, C. Jet Breakup and Spray Formation in a Diesel Engine. *Proc. Second MIT Conference on Computational Fluid and Solid Mechanics.*

[2] MacPhee, A.G., Tate, M.W., and Powell, C.F. X-ray imaging of shock waves generated by high pressure fuel sprays. Science **295:** 1261-1263 (2002).

[3] Quantitative measurement of a diesel spray core using synchrotron x-ray. In *Eighth International Conference on Liquid Atomization and Spray Systems, Pasadena, CA,* 2000.

[4] Powel, C.F., Yue, Y., Poola, R., and Wang, J. Time resolved measurements of supersonic fuel sprays using synchrotron x-rays. J. Synchrotron Rad. **7:** 356-360 (2000).

[5] Powel, C.F., Yue, Y., Poola, R., Wang, J., Lai, M., and Schaller, J. Quantitative x-ray measurements of a diesel spray core. In *Proc. 14th Annual Conference on Liquid Atomization and Spray Systems (ILASS), Dearborn, MI*, 2001.

[6] Glimm, J., Li, X.-L., and Xu, Z. Front tracking algorithm using adaptively refined meshes. *Proceedings of the 2003 Chicago Workshop on Adaptive Mesh Refinement Methods*, the Lecture Notes in Computational Science and Engineering, ISSN: 1439-7358.

[7] Glimm, J., Kim, M.-N., Li, X.-L., Samulyak, R., and Xu, Z.-L. Jet simulation in a diesel engine. *Proc. Third MIT Conference on Computational Fluid and Solid Mechanics.* 2004. Submitted.

4.3.2 TSTT: Frontier-Lite

X. Li, Z. Xu, and B. Fix

The front tracking code FronTier has been reorganized into three packages or libraries:

* A geometry package
* A dynamics package
* A physics (CFD) package

This modularization greatly increases the ease of use and ease of adoption by others, and it supports the TSTT modular interface calling conventions. The change supports our increased level of collaborations with the code development programs of other groups. Specifically we used the dynamics package in collaboration with a forest fire modeling program of David Keyes. The code merge took one afternoon. We are also using the dynamics package to model biofilm growth in collaboration with Harold Trease of PNNL. Using the package, comparison to level set methods is

routine. In Figure 11, we show the results of one rotation of a slotted disk. The FronTier solution is essentially perfect, while the level set solution fills in the slot after one quarter of one rotation. In Figure 12, we repeat this test using higher order methods and more rotations.

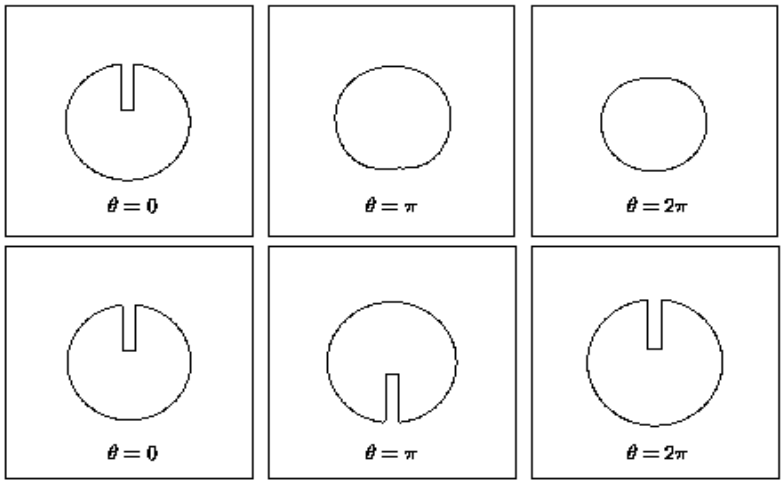

Figure 11. 1st order level set (above) compared to 1st order FronTier (below) for rigid single rotation of a slotted disk

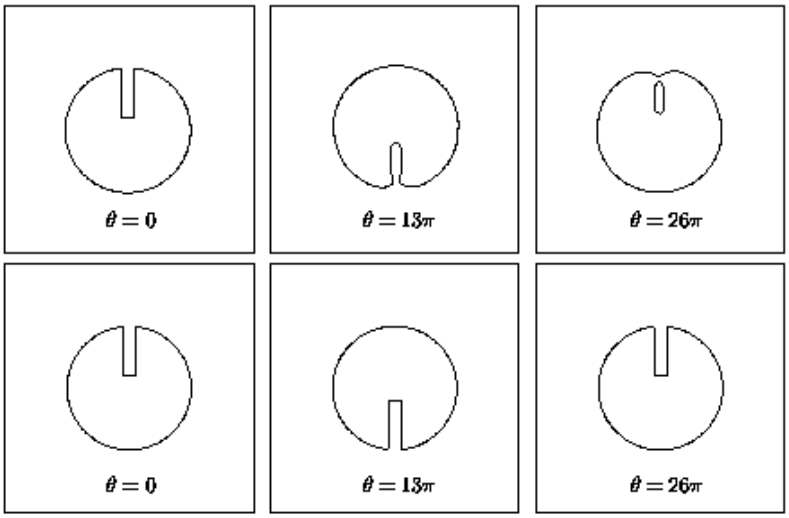

Figure 12. Level set using 5th order WENO (above) compared to 4 th order FronTier (below) for rigid 13 rotations of a slotted disk.

The physics (CFD) package has been merged with the Sandia code Qacina and the LLNL code Overture. Both codes were tested on fluid mixing problems. The Overture merge adds an AMR capability. The Qacina merge was accomplished in about two months in a collaboration of X.L. Li, Mark Christon and a Stony Brook student, Brian Fix.

Two new capabilities have been added to FronTier: Conservative tracking, which is also higher order accurate including the tracked discontinuity fronts, and a greatly improved algorithm for bifurcation and untangling of tracked fronts: local grid based tracking [1,2]. These algorithms, especially the second, are used in our ongoing studies of Rayleigh-Taylor and Richtmyer-Meshkov mixing [4, 5, 6, 7, 8].

In Figure 13, we show preliminary results from a study of a Type Ia supernova explosion. This is joint work with Srabasti Dutta and Yongmin Zhang (Stony Brook).

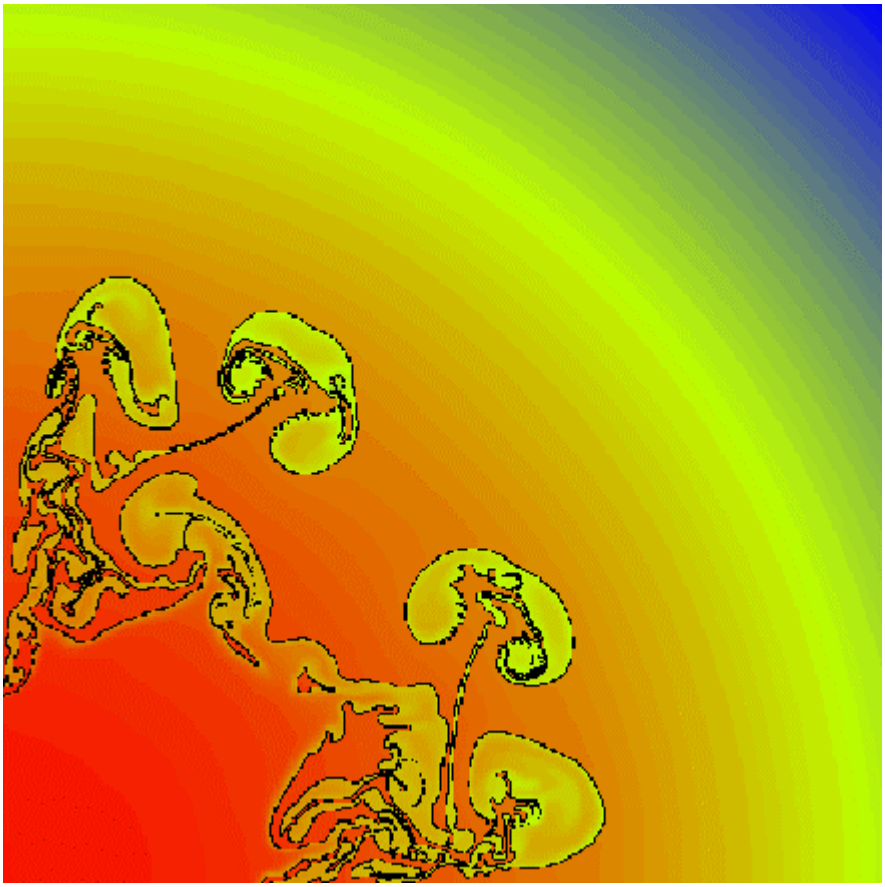

Figure 13. Color plot shows density at late time in the explosion.

References

[1] George, E., Glimm, J., Grove, J.W., Li, S.L., Liu, Y.J., Xu, Z.L., and Zhao, N. Simplification, conservation and adaptivity in the front tracking method. In T. Hou and E. Tadmor, Editors, *Hyperbolic Problems: Theory, Numerics*, Applications, pages 175-184. Springer Verlag, Berlin and New York, 2003.

[2] Glimm, J., Li, X.L., and Liu, Y.J. Conservative front tracking with improved accuracy. SIAM J. Numerical Analysis **41**, 1926-1947, 2003.

[3] Li, L., Glimm, J., and Li, X.L. All isomorphic distinct cases for multi-component interfaces in a block. J. Compl. Appl. Mathematics **152:** 263-276, 2003.

[4] George, E. and Glimm, J. Self similarity of Rayleigh-Taylor mixing rates. Phys. Fluids, submitted, 2004. Stony Brook University Preprint number SUNYSB-AMS-04-05.

[5] Jin, H., Glimm, J., and Sharp, D.H. Two-pressure two-phase flow models. ZAMP, submitted, 2003. Stony Brook University Preprint number SUNYSB-AMS-03-16 and Los Alamos National Laboratory LAUR Number LA-UR-03-7279.

[6] Zhang, Y., Drake, P., Glimm, J., Grove, J., and Sharp, D.H. Radiation coupled front tracking simulations for laser driven shock experiments. J. Nonlinear Analysis, submitted, 2004. LANL Report No. LA-UR-04-2381.

[7] Dutta, S., Glimm, J., Grove, J.W., Sharp, D.H., and Zhang, Y. Spherical Richtmyer-Meshkov instability for axisymmetric flow. Mathematics and Computers in Simulations, **65**: 417-430, 2004. University at Stony Brook Preprint number AMS-03-13.

[8] Glimm, J., Jin, H., and Zhang, Y. Front tracking for multiphase fluid mixing. In A.A. Mammoli and C.A. Brebbia, Editors, *Computational Methods in Multiphase Flow II*, pages 13-22. WIT Press, Southampton, UK, 2004.

4.3.3 Magnetohydrodynamics of Multifluid Systems

R. Samulyak, J. Glimm, Y. Prykarpatskyy, and W. Oh

Development of models, algorithms, and computational software. The purpose of this project is the development of mathematical models, numerical algorithms, and computational software for complex free surface magnetohydrodynamic (MHD) flows of conducting liquids and partially ionized plasmas in the presence of phase transitions and numerical simulations of MHD processes in several challenging DOE application areas.

The numerical simulation of complex MHD flows is a challenging problem involving mathematical modeling, development of numerical algorithms, and large scale computing. The most important modeling problems related to targeted applications are the description of thermodynamic and mechanic properties of materials interacting with intense sources of external energies. These problems include nonlinear wave phenomena, cavitation or, more generally, phase transitions in fluids, the ablation of solids by intense laser or electron beams, and atomic processes (ionization, dissociation and recombination) in gases (see Sections 4.4.4 and 4.4.5 for more details on cavitation and ablation models). The numerical problems are associated with solving of coupled hyperbolic, elliptic, and parabolic systems with strong changes in material properties along geometrically complex surfaces (free surface fluids with complex interfaces and plasmas with strong gradients/discontinuities of physical properties). The numerical technique for solving MHD equations for free surface flows is based on the method of front tracking. The front tracking for resolving discontinuities and their topological changes in hyperbolic systems has been implemented in the FronTier code. We have recently developed the corresponding methods for

elliptic systems based on finite element discretization on grids dynamically conforming to the moving interface. Scalable parallelism uses direct methods to solve the elliptic or parabolic term on each processor and an iterative technique for ensuring matching conditions across processor domain boundaries. We have also been developing an elliptic solver for FronTier-MHD based on the embedded boundary methods which is expected to be advantageous for highly complex interfaces.

Applications

Targets for Advanced Accelerators. The design of liquid mercury targets able to generate high-flux beams is among the most important problems of the design of advanced accelerators such as the Muon Collider / Neutrino Factory, and the Spallation Neutron Source. Large-scale numerical simulations of hydro and MHD processes in mercury are critical for improving the target design and reducing the number of costly experiments. The Muon Collider target has been proposed as a pulsed jet of mercury interacting with strong proton beams in a 20 Tesla magnetic field. Using the FronTier-MHD code, we have been studying surface instabilities and breakup of the mercury jet in the presence of cavitation and the stabilizing effect of the magnetic field [1,2] (see Section 4.5.1 for details).

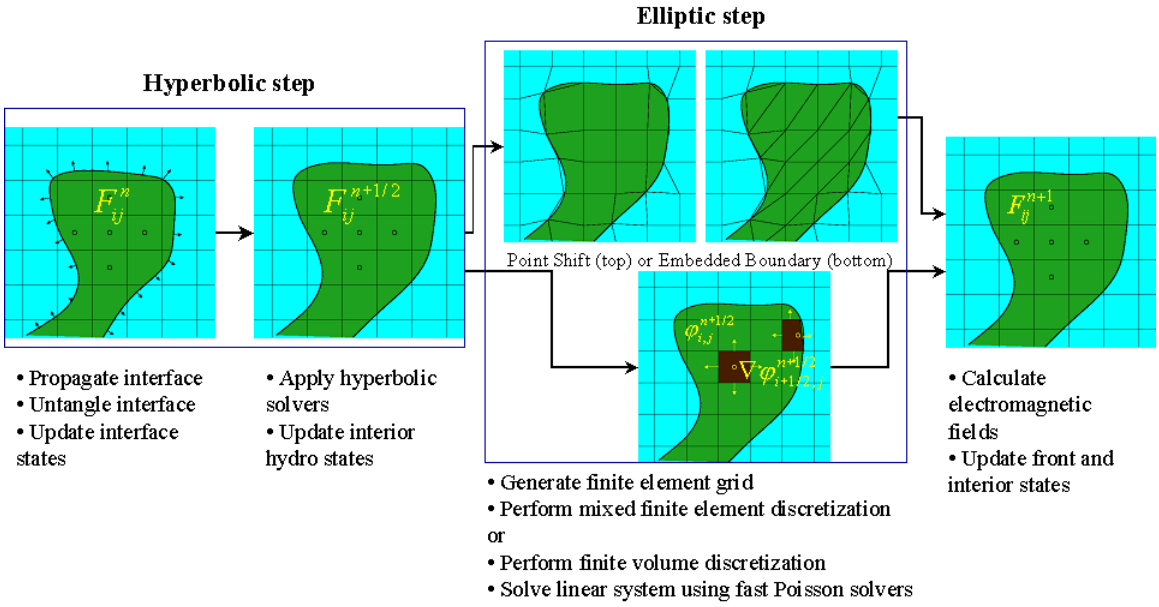

Figure 14. FronTier-MHD numerical scheme.

Laser ablation plasma plumes. Plasma plumes created by pulsed intensive laser beams can be used in a variety of technological processes including the growth of carbon nanotubes and high-temperature superconducting thin films. We have applied models for the surface ablation developed in the FronTier code to the study of the dynamics of laser ablated targets [3] and obtained a good agreement with experiments. We have also adapted our MHD models for regimes of weakly ionized plasmas and studied numerically MHD effects in ablated plumes. We have demonstrated a strong influence of the magnetic field on the evolution and parameters of ablated plumes [3] (Figure 15).

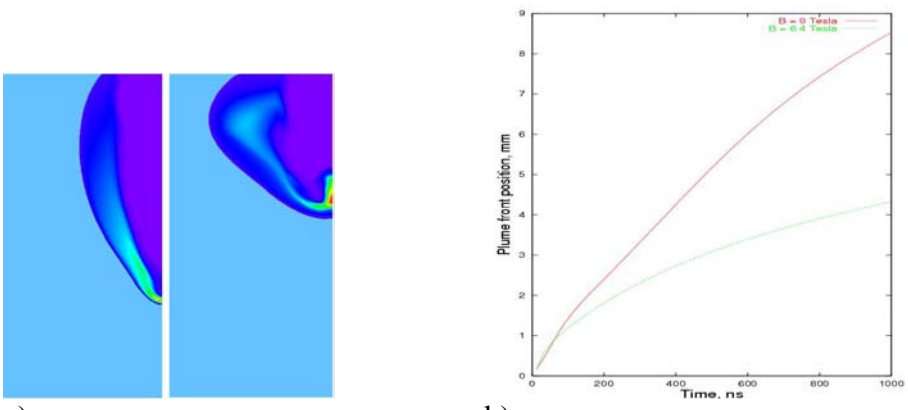

a) b)

Figure 15. Influence of the transverse magnetic field on the evolution of the silicon plasma cloud ablated by a 25 MW laser pulse. a) Density distribution at 500 ns. Left: B = 0, right: B = 6 T. b) Evolution of the plume front.

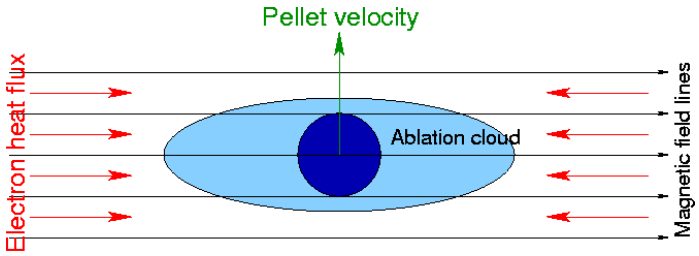

Figure 16. Schematic of processes associated with the ablation of a hydrogen pellet in tokamak.

Tokamak refueling through the pellet injection. The injection of frozen pellets of deuterium and tritium proposed is considered as the major mechanism for refueling of nuclear fusion reactors of the tokamak configuration. This problem is significantly important for U.S. fusion facilities and ITER. The schematic of a pellet in a tokamak is shown in Figure 16. Despite broad modeling and simulation efforts, currently i) there is no an accurate and complete numerical model for processes associated with the ablation of hydrogen pellets in tokamaks; ii) MHD codes for tokamak plasma simulation need an improved model for the pellet ablation. We have been working on the development and validation of such a 3D model which includes the details of the surface ablation, atomic physics effects in the ablatant plasma, and MHD. We will study the influence of various conditions on the surface ablation rate and the evolution of the ablated material, and perform simulations in the parameter regime of U.S. facilities and ITER. As a longer research effort, we will couple the developed model with MHD codes for the tokamak simulation.

References

[1] Samulyak, R., and Prykarpatskyy, Y. Richtmyer-Meshkov instability in liquid metal flows: influence of cavitation and magnetic fields. Mathematics and Computers in Simulations **65:** 431-445 (2004).

[2] Samulyak, R., Glimm, J., Oh, W., Kirk, H., and McDonald, K. Numerical Simulation of Free Surface MHD Flows: Richtmyer - Meshkov Instability and Applications, Lecture Notes in Comp. Sci. **2667:** 558-567 (2003).

[3] Samulyak, R. and Prykarpatskyy, Y. Dynamics of laser ablation plumes in magnetic fields: modeling and simulations. Physics of Plasmas (2004). Submitted.

4.3.4 ViStA: Visual Statistical Analyzer

K. Mueller and W. Zhu

It is well known that once the data become too large in size and/or dimensionality, automated data mining approaches begin to fail. To address these shortcomings, our current efforts target a classify-refine mechanism that inserts the scientist into a tight loop in the data mining process. Interaction with the system is very natural and intuitive, since the user may reorganize, restructure, or fine-tune certain components of the model or portions of the data directly within the visual display. The changes in the data organization or model are promptly recognized by the statistics engine, which then performs the necessary parameter adjustment/tuning to reflect the changes made by the user. Subsequently, a new data organization or model is computed and presented visually to the user, who may then opt to begin a new iteration cycle. Both our SpectrumMiner (Sections 4.2.3) and our BrainMiner applications use this paradigm with great success. Future work will also use this paradigm in our proteomics analysis (Section 4.4.2). In essence, ViStA is the general framework within which all of the different mining tools are unified. In the following we shall give a few examples of the visual tools that are currently available.

Viewing in the native domain. We have developed a 3D visualization interface that displays correlational data in the native domain. This tool is currently mostly used within the BrainMiner project, where the data and the functional relationships implied by the data are displayed within the brain anatomy. The correlation matrix is a 6-D object and a workable tool for its visualization is a challenge. With user selection of a single row or column, the problem reduces to three-dimensional visualization. For the brain function correlation matrix, these data are presented, along with an MRI volume and a digitized version of the Talairach brain atlas. Both can be sliced in three orthogonal directions and can be overlaid on each other. A basic view with a few regions of interest (ROIs) is shown in Figure 16, which shows the Graphical User Interface (GUI) of our newly developed 3D brain visualization software, along with a basic view of a small number of ROIs embedded into a cut-out area of a normalized/standardized MRI brain. Similar to the 2D viewer, the colors of the ROIs denote the strength of the correlational relationship, on a rainbow scale. The root ROI is colored in yellow. The GUI allows the user to slide the cutting planes up and down and back and forth, to rotate the volume, and to select certain brain surfaces, such as white matter, gray matter, and skull, to be semi-transparently superimposed. The correlation thresholds can also be selected, and many more features are available. The number of ROIs to be displayed, however, can become quite large (about 120-140), which poses challenging problems in the visualization task: in a space too crowded with statistically significant ROIs it becomes very hard, if not impossible, for the user to tell the 3D positions of the individual ROIs. To overcome these difficulties, a number of techniques [1-2] were devised, some of which are illustrated and described in Figure 17.

Viewing in an abstracted feature domain. An alternative way to view and edit causal and hierarchical relationships is in a complementary abstracted feature-centric display. We illustrated this type of display in Section 4.2.3 by way of our SpectrumMiner domain application, but similar strategies will also be available to edit causal models for our BrainMiner domain applications. A particular challenge is imposed by time-varying data. Our interactive dendrogram viewer provides the following two mechanisms to cope with this kind of data: (i) the 4D time-slice selector and (ii) the 3D ThemeRiver. We shall describe these two displays in turn.

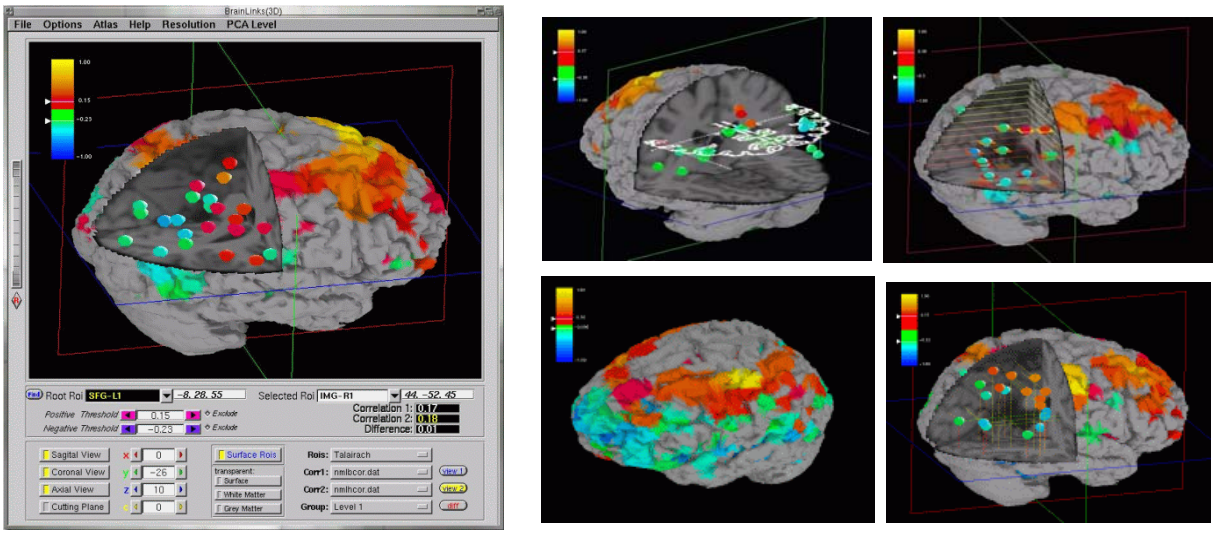

Figure 17. (*Left*) The present 3D visual interface of BrainMiner, along with a basic view of a small number of ROIs embedded into a cut-out area of a normalized/standardized MRI brain. The colors of the ROIs denote the strength of the correlational relationship, on a rainbow scale. The root ROI is colored in yellow. A legend is shown on the left to illustrate the color mapping. The two pointers in the legend can be used to select the range of statistical significance. Only ROIs within that range are displayed. The GUI also allows the user to slide the cutting planes up and down and back and forth, to rotate the volume, and to select certain brain surfaces, such as white matter, grey matter, and skull, to be semi-transparently superimposed. The correlation thresholds can be selected by moving the pointers in the color bar in the upper left corner of the display. When the sliders are moved, the application adjusts the color range such that the entire range of rainbow colors is always utilized. Two studies (baseline and drug) can be loaded simultaneously. The display can then be switched between three correlation matrices: those of the two loaded studies as well as the difference correlation matrix. The latter display shows the ROIs that have changed, under the influence of the drug, their statistical relationship with respect to the selected root ROI; (*center column top:*) superimposing a Talairach atlas slice (or an MRI slice) that can be slid up and down the volume; (*right column top:*) enhancing the ROIs by colored halos or coasters, where the colors code their height and depth on a rainbow color scheme, to aid the perception of 3D depth relations; (*center column bottom*:) near cortex ROI-correlations projected onto the cortex surface; (*right column bottom*:) depth cues provided drop lines.

The 4D time-slice selector. The interactive dendrogram represents time-varying data as a cylindrical shape composed of a stack of circular time-slice dendrograms. The time-slice selector shown above the dendrogram in Figure 17 shows the unwrapped outer surface of this cylinder, with each horizontal slice capturing the leaf nodes of one time-slice dendrogram. Patterns in the data distribution over time are clearly visible. Stepping across the time slices will animate the data-related coloring of the dendrogram's arcs.

The 3D ThemeRiver. To show the fluctuations of different variables (i.e., nodes in the time-varying dendrogram) over time, we use the ThemeRiver paradigm [3] that visually illustrates multiple variables as parallel streams in which the width of the stream maps to node magnitude. A limitation of the existing ThemeRiver scheme is that only one attribute can be displayed per theme. We therefore have devised a 3D extension, which enables us to display two attributes of each variable in the data stream. The new 3D ThemeRiver [4] can display any ternary relationships within the data, and not just as a function of time. The surface itself is modeled as a smooth 3D Bezier mesh, where constraints have been added to prevent overshoot at extreme points of the dependent variables. Users can draw any free-hand curve into the dendrogram, which maps the nodes above the intersected edges as streams into the 3D ThemeRiver window (see Figure 18).

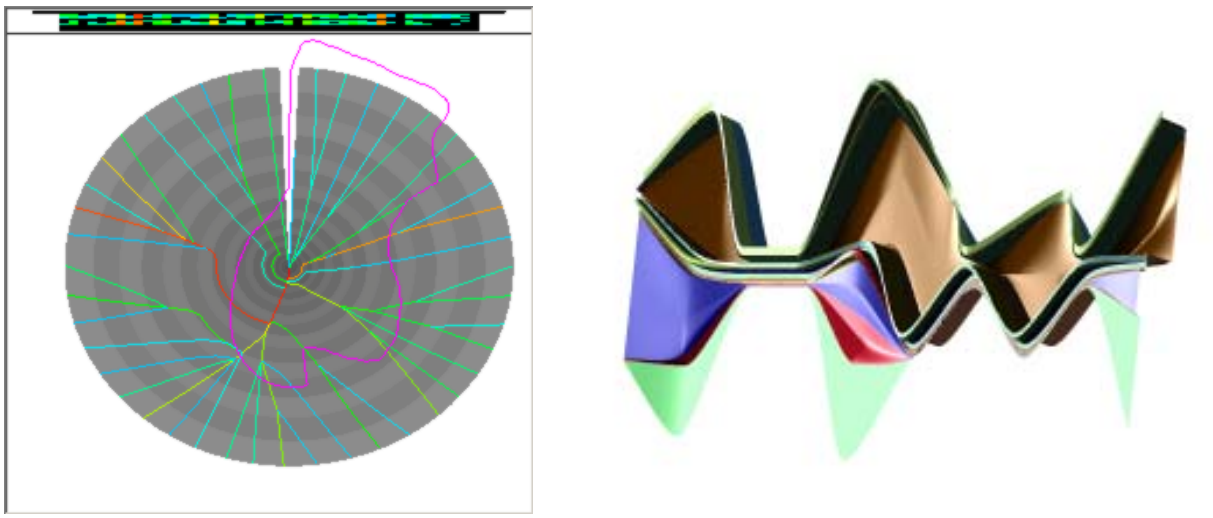

Figure 18. Left: The dendrogram with a user-drawn closed freeform line specifying the time axis-centric surface to be visualized with 3D ThemeRiver. Right: A 3D ThemeRiver visualization of 17 clusters of organic aerosols. Width encodes overall cluster distribution and the height encodes incidence of zinc. The horizontal axis represents the increasing concentrations of ozone in the atmosphere.

Focussed viewing while preserving visual context. In the dendrogram, a number of features are available to enable focus with context, including collapsible sub-trees and node coalescing, search by label and feature, node-content browsers, and non-linear rubber-sheet distortion using an interactive, graphics-hardware-accelerated technique (see Figure 19) [4].

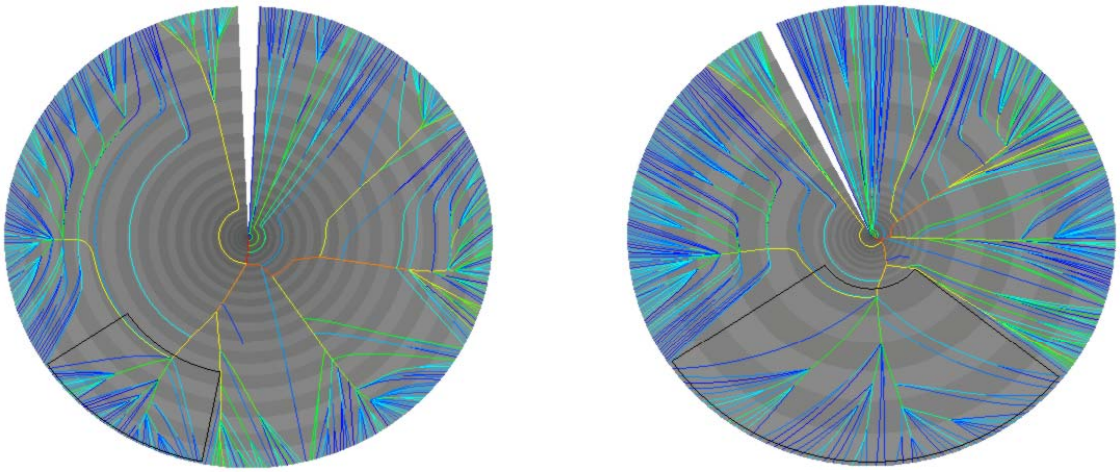

Figure 19. Rubbersheet zooming. Left: unwarped dendrogram; Right: a user-specified arc segment (shown as a black-framed area) is angularly expanded and radially shrunk. Notice the radial distortion of the dendrogram's polar rings.

References

[1] Mueller, K., Welsh, T., Zhu, W., Meade, J., and Volkow, N. Brain Miner: A Visualization Tool for ROI-Based Discovery of Functional Relationships in the Human Brain, *New Paradigms in Information Visualization and Manipulation (NPIVM) 2000*, Washington DC, November 2000.

[2] Welsh, T., Mueller, K., Zhu, W., Volkow, N., and Meade, J. Graphical strategies to convey functional relationships in the human brain: A case study. *Visualization '01*, pp. 481-485, San Diego, October 2001.

[3] Havre, S., Hetzler, E., Whitney, P., and Nowell, L. ThemeRiver: Visualizing thematic changes in large document collections. IEEE Trans. Visualization and Computer Graphics **8(1):** 9-20 (2002).

[4] Imrich, P., Mueller, K., Imre, D., Zelenyuk, A., and Zhu, W. Interactive Poster: 3D ThemeRiver. IEEE Information Visualization Symposium '03, October 2003.

[5] Imrich, P., Mueller, K., Imre, D., Zelenyuk, A., and Zhu, W. Interactive Poster: A hardware-accelerated rubbersheet focus+context technique for radial dendrograms. IEEE Information Visualization Symposium'03, October 2003.

4.3.5 Uncertainty Quantification

J. Glimm

Quantification of Uncertainty and Computer Assisted Decision Making

The need for computer assisted decision making is driven by two related factors. The first is the importance of complex scientific/technical decisions, such as those related to global warming, for

which controlled experiments are not feasible. The second is the need for rapid or timely decisions, using incomplete information, such as in shortening the time to market duration of a product design cycle, mandating a reduction of the role of the human in the loop.

A key issue, and the central one considered here, is an accurate assessment of errors in numerical simulations [1]. Errors are assessed statistically, based on a formula

error = exact solution - approximate solution

The essential difficulty is that an "exact" or sufficiently improved solution requires more resources, as does the ensemble needed to characterize the error statistically. Similarly, the dependence of the error statistics on the problem parameters adds to the resource requirements.

Fortunately, we have developed several approaches to mitigate this UQ-explosion of resource requirements.

We have shown that linear models may be sufficient to describe errors even for deeply nonlinear problems [3]. We have shown that complex problems can be decomposed, and models for the total error can be expressed as a composition of error models for each of the components [4,5,6].

We have shown that the dependence of errors on parameters can be expressed in linear regression models [1] and that total prediction errors can to attributed quantitatively to prediction errors ascribed to various sources (data insufficiency, inverse problem error, forward simulation error, ...) [4]. Dependence of the solution error on the numerical algorithm is studied in [2].

In general, we have used simple Gaussian models to express solution error, characterized by the mean and covariance. Because the solution is a field quantity (depending on time, space variables) this error is a field quantity also. With limited data on the solution error, it is desirable to reduce the dimension of the error mean and covariance. The reduction is problem dependent, but an interesting outgrowth, in our shock physics applications, has been a wave filter post processing algorithm to identify, locate, and label shock and contact waves in a shock wave interaction problem [3].

We have also used these tools to compare different algorithms. For example, we find that use of Front Tracking reduces the error in a simple spherical implosion or explosion problem by an amount equal to mesh refinement to a factor of 4 to 8 per linear dimension [2].

References

[1] Glimm, J., Hou, S., Lee, Y.-H., Sharp, D.H., and Ye, K. Solution error models for uncertainty quantification. Contemporary Mathematics **327:** 115-140 (2003).

[2] Dutta, S., Glimm, J., Grove, J.W., Sharp, D.H., and Zhang, Y. Error comparison in tracked and untracked spherical simulations. Computers and Mathematics with Applications. In press (2004).

[3] Glimm, J., Grove, J.W., Kang, Y., Lee, T.W., Li, X., Sharp, D.H., Yu, Y., Ye, K., and Zhao, M. Statistical Riemann problems and a composition law for errors in numerical solutions of shock physics problems. SISC. In press (2004).

[4] Glimm, J., Hou, S., Lee, Y., Sharp, D.H., and Ye, K. Sources of uncertainty and error in the simulation of flow in porous media. Comp. App. Math. In press (2003). SUNYSB-AMS-03-08.

[5] Glimm, J., Grove, J.W., Kang, Y., Lee, T., Li, X., Sharp, D.H., Yu, Y., and Zhou, M. Errors in numerical solutions of spherically symmetric shock physics problems. Cont. Math. In press (2004).

[6] Lee, T., Yu, Y., Glimm, J., and Ye, K. Error analysis of composite shock interaction problems. Proc. PMC04, 2004.

4.3.6 Visualization

R. Bennett, M. McGuigan, G. Smith, J. Spiletic, and S. Tomov

Parallel visualization allows one to handle scientific data sets that are too large or render too slowly on single processor systems. In [1] we implemented interactive parallel visualization by extending popular APIs such as Open Inventor and VTK to support commodity-based clusters. In this work we used Chromium, a popular software tool that provides scalable display technology, to implement our parallel rendering. Figure 20 shows a result from the parallel visualization on four processors of an X-ray tomograph taken of the thigh bone of a rat used in osteoporosis studies. The different colored isosurfaces are handled by separate processors.

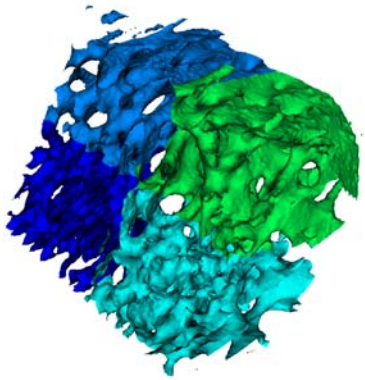

Figure 20. Parallel visualization of the thigh bone of a rat used in osteoporosis studies.

The high performance (40Gflops peak) and low cost ($400) of current graphics cards have given rise to great interest in using Graphics Processing Units (GPUs) for non-graphics scientific computations. In [2] probability-based simulations were implemented on the GPUs and their performance was benchmarked and compared against the CPU with an overall 3 times speedup for the GPU. Such probability-based simulations have a wide range of applications in physics, biology, chemistry and finance. They are computationally intensive and lend themselves naturally

to lattice implementations on GPUs. Specifically we demonstrate the techniques using Monte Carlo simulation of the Ising spin model used in physics to study phase transitions in magnetic materials. The GPU Monte Carlo implementation used Cg (C for graphics) fragment programs, which are executed on the GPU by an OpenGL application. We use a standard "Dynamic texturing" programming model, where the computational domain is modeled by a texture, then a GPU fragment program uses the texture to render an image in an off-screen buffer, and finally the texture is updated from the resulting image. Special care is taken (on algorithmic and data representation level) to organize the computations in terms of 4D vector operations, which is important in the current GPUs in order to extract maximal performance. Figure 21 shows a direct visualization and computation on the graphics card of the 3D Ising model with red indicating spin up and blue spin down.

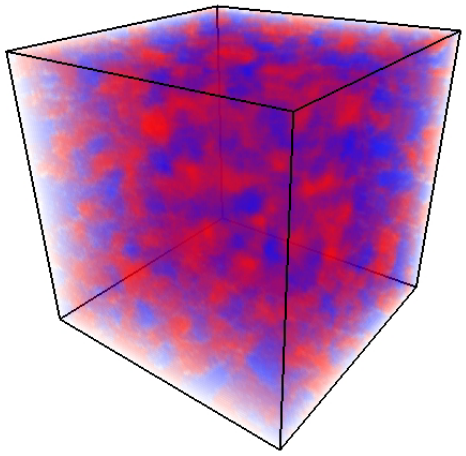

Figure 21. Graphics card computation of 3D Ising model.

References

[1] Tomov, S., Bennett, R., McGuigan, M., Peskin, A., Smith, G., and Spiletic, J. Application of interactive parallel visualization for commodity-based clusters using visualization APIs . Computers & Graphics **28(2):** 273-278 (2004).

[2] Tomov, S., McGuigan, M., Bennett, R., Smith, G., and Spiletic, J. Benchmarking and implementation of probability-based simulations on programmable graphics cards. Computers & Graphics **29(1)**, February 2005.

4.3.7 Cluster Computing

N. D'Imperio and E. McFadden

Linux clusters have become important providers of computing cycles in the scientific world. (http://www.ccd.bnl.gov/bcf/cluster/). The CSC cluster, named Galaxy, consists of 256 Intel P3 and P4 processors running at speeds up to 2.4 GHz. Arranged in dual processor nodes, most have 1 Gbyte of memory per node. A RAID storage facility with 1.4 terabytes of disk is attached to this machine. Parallel computations are performed using the message passing interface, MPI (www-unix.mcs.anl.gov/mpi) and through threads using Open MP.

Our goal is to continue to explore the frontier of the commodity component world, as processor, motherboard bus, and memory speeds increase, as fiber cable decreases in price, and as switch speeds increase in performance and decrease in price. We will determine optimal configurations and architectures, within the overall framework of our design. Results from this research will be published and posted on the network, to benefit others seeking a similar price/performance advantage.

The Galaxy computer provides computing cycles to CSC affiliates and projects. Convenient and assured access to local parallel computing is an essential requirement for the development of parallel simulation codes, and it is thus a key component of the CSC strategy to make state-of-the-art computing technology available to benefit BNL scientific programs.

4.4 BASIC ENERGY SCIENCES

The Department of Energy's Office of Basic Energy Sciences supports research in materials and chemical sciences, geoscience, engineering, and energy biosciences. This broad-based program of fundamental research is also responsible for a number of national user facilities, including synchrotron x-ray and neutron sources and electron microscope facilities. CSC has engaged in numerous projects in computational fluid dynamics, many body physics, and optics, which are described here. Most projects are in collaboration with BES scientists and support the BES missions.

4.4.1 Superconductivity: Charge Distribution in the Superconductor Magnesium Diboride

J. Zheng, J. W. Davenport, and Y. Zhu

MgB_2 has recently been found to display superconductivity at the surprisingly high temperature of 39K [1]. This fact has stimulated a large research effort to determine the cause of the high transition temperature, as well as other properties of this otherwise unremarkable material. We have utilized first principles density functional theory to calculate the charge density in MgB_2 and compare it with transmission electron microscope and synchrotron x-ray measurements carried out at Brookhaven. We used the full potential linear augmented plane wave (FLAPW) method to solve the density functional equations [2]. The calculated lattice constants are in good agreement with previous calculations and with experiments. The same technique had been used earlier to study the distribution in energy of the occupied and empty states [3].

MgB_2 forms in a hexagonal crystal structure, with the boron atoms arranged in a honeycomb fashion in planes that are structurally the same as graphite. The magnesium atoms are located in the hollow positions in parallel planes above and below.

Figure 22 shows a contour plot of the difference charge density in the boron plane [4]. The difference density is obtained by subtracting the density of isolated atoms from that of the compound. The red areas between the atoms show clearly the build up of the bond charge.

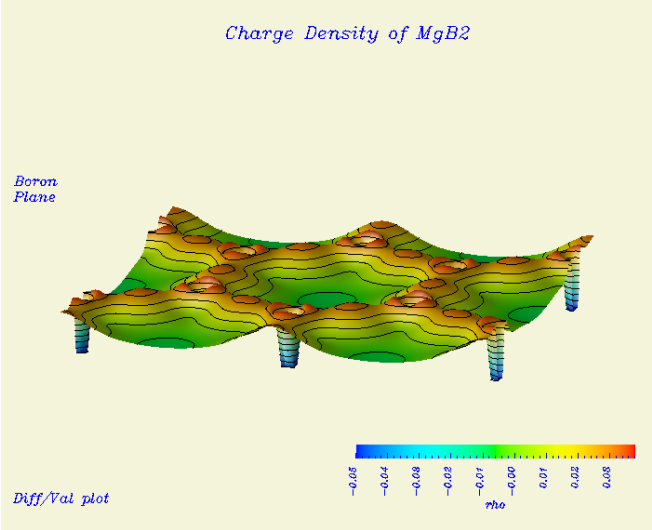

Figure 22. Charge density contours in the hexagonal compound MgB_2 calculated from first principles density functional theory.

Experiments measure the structure factors of the charge distribution, which are related to the Fourier transform of the density. The calculations described here agree with the experiments to within 3%. Calculations using only the atomic density, which are typically used in diffraction experiments, disagree with the data by up to 28%, clearly showing the importance of quantum mechanical calculations of x-ray diffraction. We have also studied the details of the x-ray absorptive edge, finding excellent agreement with experiments [5,6].

References

[1] Nagamatsu, J., Nakagawa, N., Muranaka, T., Zenitani, Y., and Akimatsu, J. Superconductivity at 39K in magnesium diboride. Nature **410**: 63 (2001).

[2] Blaha, P., Schwarz, K., Madsen, G., Kvasnicka, D., and Luitz, J. WIEN2k, an augmented plane wave + local orbitals program for calculating crystal properties (Karlheinz Schwarz, Techn. Universitat Wien, Austria), 2001. ISBN 3-9501031-1-2.

[3] Zhu, Y., Moodenbaugh, A. R., Schneider, G., Davenport, J. W., Vogt, T., Li, Q., Gu, G., Fischer, D. A., and Tafto, J. Unraveling the symmetry of the hole states near the Fermi level in the MgB2 superconductor. Phys. Rev. Lett. **88:** 247002 (2002).

[4] Wu, L., Zhu, Y., Vogt, T. Su, H., Davenport, J. W., and Tafto, J. Study of valence electron distribution in MgB_2 by accurate diffraction measurements and first principles calculations. Phys. Rev. B. Submitted.

[5] Moodenbaugh, A.R., Fischer, D.A., Li, Q., Gu, G., Zhu, Y., Su, H., Welch, D.O., and Davenport, J.W. X-ray absorption study of the boron K near edge in MgB_2. Submitted.

[6] Klie, R.F., Su, H., Zhu, Y., Davenport, J.W., Idrobo, J.-C., Browning, N., and Nellist, P.D. Measuring the hole-state anisotropy in MgB_2 by electron energy-loss spectroscopy. Phys. Rev. B **67:** 144508 (2003).

4.4.2 Scalable Localizable Density Functional Theory

J. Davenport, D. Volja, J. Zheng, K. Kang, and D. Keyes

Nanoscale science and technology and biology are driving a search for new ways to calculate the electronic properties of clusters containing many thousands of atoms. Density Functional Theory (DFT) has been shown to yield accurate total energies, charge, and spin densities in molecules and crystalline solids but has been limited in the size system that can be treated.

The density functional equations consist of coupled Schrodinger and Poisson equations, which must be solved self consistently. Usually one chooses a basis set (for example Gaussian type orbitals or plane waves) thereby converting the Schrodinger equation into an algebraic eigenvalue problem. The number of such basis functions will scale linearly with N, the number of atoms in the system. Solving the eigenvalue problem, which is formally dense, will then scale as N^3. Hence for large systems, there is a premium on efficiency, or reducing the number of basis functions required per atom. Gaussian type orbitals (GTOs) have the advantage of being highly localized in space, decaying like $\exp(-ar^2)$. However, they are not maximally efficient, in the sense that many Gaussians are required to accurately represent the wave functions. Plane waves have the disadvantage that they are not localized at all, but rather extend over the whole system. In addition their use generally requires a "supercell" in which the system is repeated periodically in space, leading to inaccurate treatment of surface and edge effects in some cases.

We solve these problems by using a mixed numerical and localized analytical basis set. We partition the space into nonoverlapping spheres surrounding each atom and an extra-atomic region outside the spheres. Inside the spheres the basis consists of numerical solutions of the Schrodinger (or Dirac) equation for the spherical part of the potential. Outside the spheres, the basis is given by Slater type orbitals, which have the form

$$\phi_{nlm}\left(\vec{r}\right) = r^{n-1}\exp\left(-\zeta r\right)Y_{lm}\left(\vec{r}\right)$$

where the Ys are spherical harmonics. These functions are not overly localized as are GTOs and achieve the same accuracy more efficiently.

At each sphere boundary these functions are matched onto the numerical solutions inside the sphere. Such a scheme has already been implemented for periodic systems and is known as LASTO, the Linear Augmented Slater Type Orbital method [1]. It is a local orbital version of the Linear Augmented Plane Wave (LAPW) method, considered the most accurate method for solving the DFT equations.

The Poisson equation is solved on a numerical grid using sparse matrix techniques and the hypre library [2]. Hypre is a set of highly parallel preconditioners and solvers suitable for large sparse

systems. The eigenvalue problem is solved using ScaLAPAK [3], a set of codes for the solution of large eigenproblems.

For the largest systems we use an O(N) technique known as "divide and conquer" [5]. In this method, a large cluster is partitioned into subsystems, and the charge density is calculated for each. The computational effort scales like SN_s^3, where S is the number of subsystems and N_s is the number of atoms in the subsystem. This scheme is possible because the charge density (more generally, the density matrix) is localized in space even when the eigenfunctions are not [6].

Using divide and conquer, along with the localized basis set provided by STOs, we expect to be able to calculate the charge and spin density of clusters containing up to 5000 atoms.

References

[1] Fernando, G.W., Davenport, J.W., Watson, R.E., and Weinert, M. Full-potential linear augmented-Slater type orbital method. Phys. Rev. B **40:** 2757 (1989).

[2] hypre, high performance preconditioners, www.llnl.gov/CASC/hypre/

[3] ScaLAPAK, http://netlib2.cs.utk.edu/scalapack/

[4] PETSc, Portable, Extensible Toolkit for Scientific Computing. www.mcs.anl.gov/petsc/

[5] Yang, W. Direct calculation of electron density in density-functional theory. Phys. Rev. Lett. **6:** 1438 (1991).

[6] Kohn, W. Density functional and density matrix method scaling linearly with the number of atoms. Phys. Rev. Lett. **76:** 3168 (1996).

4.4.3 Prediction of Surface Magnetism in Uranium Metal

N. Stojic, J. Davenport, and J. Glimm

Uranium, the heaviest naturally occurring element, has been studied for many years. Metallic uranium has an interesting complex crystal structure, as is shown in Figure 23. It is the only nonmagnetic element known to form an incommensurate charge density wave state at low temperatures. At room temperature it crystallizes in an orthorhombic structure, and on heating passes through tetragonal and body centered cubic (bcc) phases before melting at 1408K. As one of the actinides, it has partially filled 5*f* states, yet unlike the 4*f* (rare earth) elements and the heavier actinides, the 5*f* electrons are believed to be relatively delocalized and contribute to the metallic bond. Many uranium alloys display heavy fermion behavior, indicating some form of incipient localization.

In this work we have used first principles density functional theory, including the spin orbit interaction, to calculate the magnetic properties of thin films [1]. We find, surprisingly, that the surfaces of the films are magnetic, even though the bulk material is not. We predict that this

magnetic surface layer is also present at the crystalline surface. We have also calculated the structural properties and bulk moduli of the competing phases. We find that the bcc phase is mechanically unstable, meaning that the energy as a function of tetragonal distortion has negative curvature. Describing the mechanical stability of nonequilibrium phases is important for phase diagram construction, the structure of grain boundaries, and epitaxial thin films.

The calculations were performed with the full potential linearized augmented plane wave method as embodied in the WIEN2k code [2]. This is widely recognized as the most accurate method for solving the density functional equations (a set of single particle equations obtained by reduction from many body problems applying the density functional theory). The WIEN2k code includes

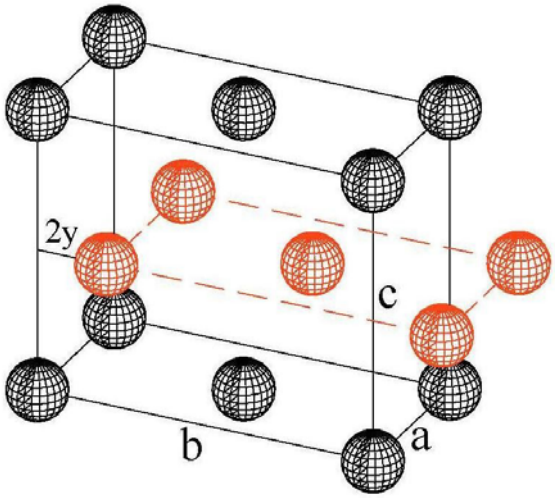

Figure 23. Alpha uranium crystal structure. a = 2.836Å, b = 5.866Å, c = 4.935 Å, y = 0.1017.

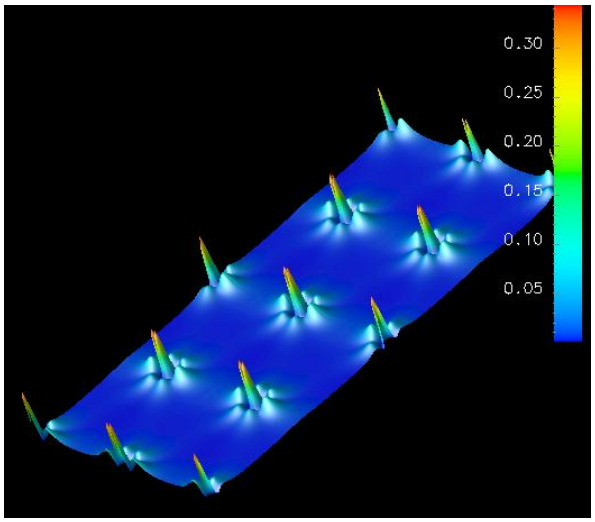

Figure 24. Calculated spin density on outer-most plane of uranium. The units are Bohr magnetons.

local orbitals to better describe semi core states. We also used the generalized gradient approximation (GGA) for exchange and correlation as described by Perdew et al. in [3]. Use of the GGA leads to a significant improvement in the calculated volume compared with experiment [4]. Structures studied included the simple, face centered, and body centered cubic, body centered tetragonal, orthorhombic, and hexagonal close packed. We determined the cohesive energy, equilibrium volume, and bulk modulus for each structure. Structural energy differences and vacancy formation energy for the BCC lattice were also found. To study surfaces, films of 1 – 7 layers were constructed in supercell geometry.

All of the films displayed large magnetic moments of approximately 0.65 Bohr magnetons per atom, concentrated in the surface plane (1 Bohr magneton is the magnetic moment of a single electron--it is noninteger in metals because of chemical bonding effects). The spin density in the outermost plane is shown in Figure 24. The multilobed angular dependence shows clearly that the moment is primarily due to the 5f electrons. We also calculated the surface and spin projected density of states and predict that the magnetic effects should be easily observable in experiments such as spin polarized photoemission or circular dichroism.

If verified, this would be only the second example found of a nonmagnetic element that possesses a surface magnetic moment and illustrates the possibility of designing completely new magnetic materials.

The mechanical instability of the bcc phase is illustrated in Figure 25, which shows the energy as a function of volume and c/a ratio for tetragonal distortions. The total energy of the bcc phase is 0.22 eV / atom above the ground state (orthorhombic) phase.

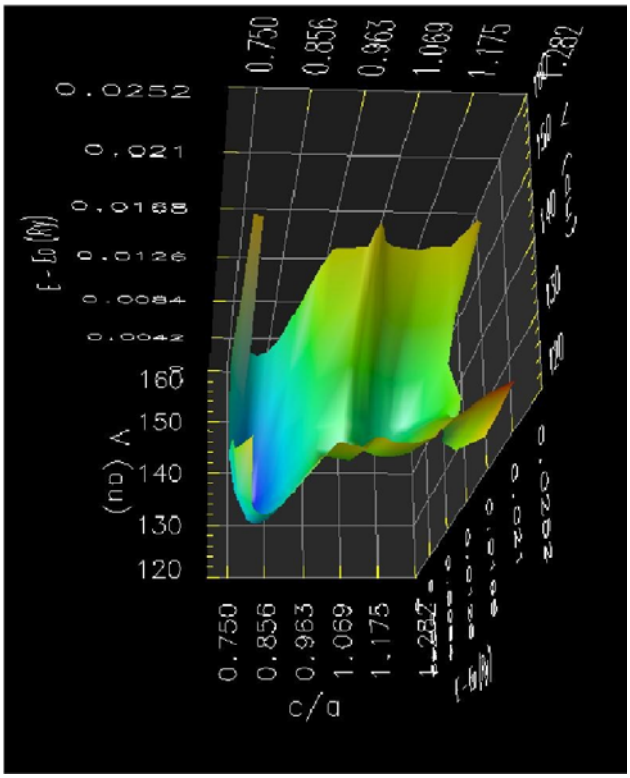

Figure 25. Mechanical instability of the BCC structure, located along the c/a= ridge above. The energy is displayed as a function of unit cell volume and ratio of lattice axes c/a. We changed the c/a ratio, thus deforming the BCC structure (c/a = 1) into a body-centered tetragonal lattice structure, which has an energy minimum at c/a = 0.8123 and V = 20.653 Å^3 (139.370 bohr^3).

References

[1] Stojic, N., Davenport, J.W., Komelj, M., and Glimm, J. Surface magnetic moment in alpha uranium by density functional theory. Phys. Rev. B **68:** 094407-1 (2003).

[2] Blaha, P., Schwarz, K., and Luitz, J. *WIEN97, A Full Potential Linearized Augmented PLane Wave Package for Calculating Crystal Properties.* (Karlheinz Schwarz, Technical Universit@t Wien, Austria, 1999). ISBN 3-9501031-0-4.

[3] Perdew, J.P., Burke, S., and Ernzerhof, M. Phys. Rev. Let. **77:** 3865 (1996).

[4] Jones, M.D., Boettger, J.C., and Albers, R.C. Phys. Rev. B **61:** 4644 (2000).

4.4.4 Cavitating and Bubbly Fluids

R. Samulyak, J. Glimm, T. Lu, Y. Prykarpatskyy, Z. Xu

An accurate description of cavitation and wave propagation in cavitating and bubbly fluids is a key problem in modeling and simulation of hydrodynamic processes in a variety of applications ranging from marine engineering to high energy physics. We are interested in the study of cavitation and bubbly fluids occurring in liquid mercury targets that interact with high intensity proton pulses. Such targets are key components of advanced accelerators such as the Spallation Neutron Source (http://www.sns.gov) and Muon Collider/Neutrino Factory (www.cap.bnl.gov/mumu).

Modeling of the cavitation is a complex multiscale and multiphysics problem involving the description of thermodynamic properties of liquids undergoing phase transitions and nonlinear wave phenomena in multiphase systems. We have been working on two different approaches to this problem. The first one (the **direct method**) is based on unique interface tracking capabilities of our hydro code FronTier. The second approach (the **homogeneous method**) is based on a continuous description of the liquid -- vapor or liquid -- non-dissolvable gas mixtures by means of homogeneous equation of state models. The two methods are complementary and can be used to resolve different spatial scales in simulations.

Direct method. In the direct method, a liquid -- vapor or liquid -- non-dissolvable gas mixture is represented as a system of one phase domains (vapor bubbles, for instance) separated by free interfaces. The FronTier code is capable of tracking simultaneously a large number of interfaces and resolving their topological changes (the breakup and merger of droplets) in two- and three-dimensional spaces. Though computationally intensive, such an approach is potentially very accurate in treating important effects in bubbly flows including bubble oscillations, heat transfer, drag, viscosity, and surface tension. The method makes it possible to resolve spatial scales smaller than the typical distance between bubbles and model some non-equilibrium thermodynamic features such as finite critical tension in cavitating liquids. Numerical simulation of the cavitation presents additional level of complexity compared to the simulation of wave phenomena in bubbly fluids (fluids containing small non-dissolvable gas bubbles). The problem is associated with the dynamic creation and collapse of bubbles in the computational domain. The corresponding numerical models and software routines have been developed and implemented in the FronTier code. To account for the phase transition induced mass transfer across the liquid - vapor interface, we have developed a nonlocal Riemann solver governing the evolution of interfaces. The direct method has been validated through the comparison of numerical simulations with theoretical predictions and classical experiments on linear (sound) and nonlinear (shock) waves in bubbly fluids [2,3] (see Figure 26) and applied to the study of the Muon Collider and Spallation Neutron Source (see Sections 4.5.1 and 4.5.4) and the liquid jet breakup and atomization (Section 4.3.1).

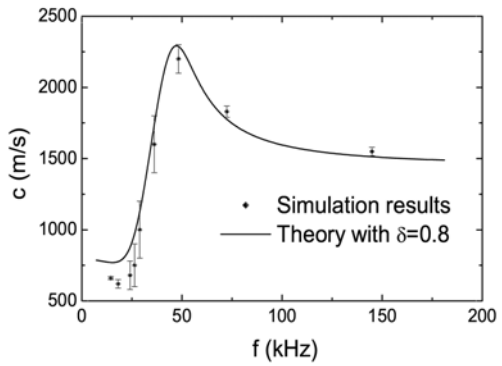

Figure 26. Dispersion relation in bubbly flows. The bubble radius is 0.12mm, void fraction is 1.5510^{-4}, and the pressure is 1.0 bar. The amplitude of the incident pressure wave is 0.1 bar. Grid size is 90 x 10800 and δ is the damping coefficient.

The current computational capabilities of our hardware allow the use of this approach for the study of wave dynamics in thin layers of bubbles in two and three dimensions. It is prohibitively expensive, however, to study large bubbly volumes by direct numerical simulations. The homogeneous approach described below is used for such systems.

Homogeneous method. The advantage of the homogeneous method compared to the direct one is its computational simplicity and, as a result, low computational requirements for the simulation of large systems. The homogeneous flow approximation provides a simple technique for analyzing two-phase (or multiple phase) flows. It is accurate enough to handle a variety of practically important processes. Suitable average properties are determined and the mixture is treated as a pseudofluid that obeys an equation of single-component flow [1].

We have developed an isentropic homogeneous equation of state for two-phase liquids and implemented the corresponding software library in the FronTier code. Due to averaging, the EOS does not resolve spatial scales comparable to the distance between bubbles. It is suitable for numerical simulations of the global dynamics of two phase domains. The code has been applied to the study of the interaction of mercury with intensive proton pulses in the geometry typical for the Muon Collider/Neutrino Factory liquid mercury target experiments carried out at the BNL AGS and CERN ISOLDE [4], and a good agreement with experimental data has been achieved [1,2] (see Figure 27).

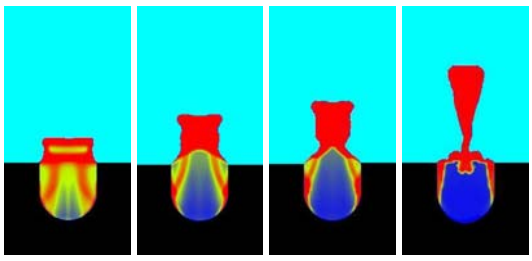

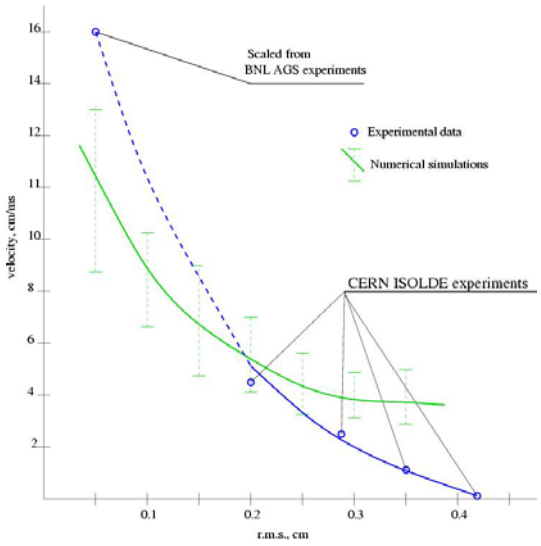

a) b)

Figure 27. Evolution of the mercury splash in a thimble due to the interaction with a proton beam (beam parameters: 24 GeV, $3.7*10^{12}$ protons). a) Numerical simulations using the FronTier code and analytical isentropic two phase equation of state. b) Surface velocity of the mercury splash in the thimble as a function of the r.m.s. spot size of the beam.

References

[1] Samulyak, R. and Prykarpatskyy, Y. Richtmyer-Meshkov instability in liquid metal flows: influence of cavitation and magnetic fields. Mathematics and Computers in Simulations **65:** 431-446 (2004).

[2] Samulyak, R., Lu, T., Prykarpatskyy, Y., Glimm, J., Xu, Z., and Kim, M.-N. Comparison of direct and homogeneous numerical approaches to cavitation modeling. Int. J. For Multiscale Comp. Eng., (2004). Submitted.

[3] Samulyak, R., Lu, T., and Prykarpatskyy, Y. Direct and homogeneous numerical approaches to multiphase flows, Lecture Notes in Comp. Sci. **3039**:653-660 (2004). Springer-Verlag, Berlin - Heidelberg, 2004.

[4] Fabich, A., and Lettry, J. Experimental Observation of Proton-Induced Shocks and Magneto-Fluid-Dynamics in Liquid Metal, In Proc. NuFact 01, NIM A, 2001.

4.4.5 Laser Ablation Plasma Plumes

R. Samulyak and Y. Prykarpatskyy

The interaction of pulsed intensive laser radiation with solid targets and the expansion of ablated plumes has recently received increased attention due to its importance in laser deposition, nanoparticle formation and growth, cluster production, etc. In addition to these applications, studies of the plume dynamics are very important for modeling of various processes in space physics, plasma chemistry, and hydrodynamics. The expansion of ablated plumes in an ambient gas is a complex process involving several physics phenomena.

In a typical laser ablation experiment for nanoparticle production, a target (aluminum or silicon) in non-reactive background gas (argon) at a low or atmospheric pressure is ablated with a laser creating a thin melted layer, a Knudsen layer [2] or a gasdynamic discontinuity layer within which the translational equilibrium is achieved through particle collisions, and a rapidly expanding vapor plume (Figure 28).

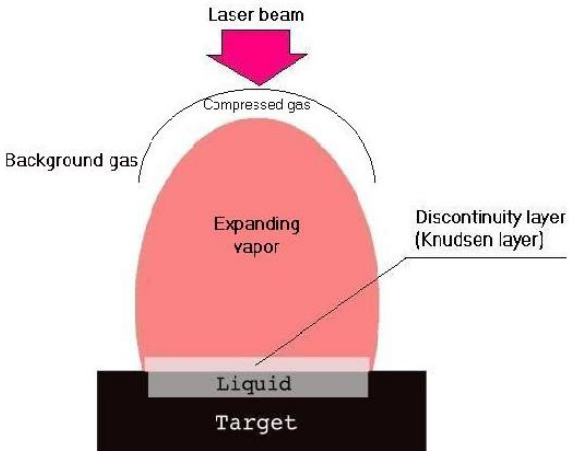

Figure 28. Schematic of processes associated with the laser ablation of a solid target.

The vapor ejected by laser radiations usually supercools because of its expansion and interaction with the cold ambient gas. The supercooled vapor condenses partially on the target surface and partially in the gas phase, in the form of nanosize particles. At high laser flux density or low ambient gas pressure, a supersonic vapor flow is formed where adiabatic expansion is the

predominant cooling mechanism. At lower laser flux densities, a subsonic vapor jet is created where where the heat conduction and diffusion mixing with the ambient gas are the predominant mixing mechanisms. The formation of nanoparticles and nanotubes depends on metal catalyst particles in the vapor.

Modeling of the ablation of solid surfaces is a coupled multiscale problem which involves the heat transport equation in the solid target, phase transition equations, equations for the Knudsen layer, and equations for the dynamics for the ablated material. The equilibrium thermodynamic description of the ablation process, namely the Clausius-Clapeyron relation and the mass transfer rate equation, can be used for practically important regimes [2]. The ablation model has been implemented in the FronTier code and applied to the study of the dynamics of laser ablation plumes in magnetic fields [3] and preliminary studies of processes associated with the ablation of hydrogen pellets in tokamaks. A simplified description of the ablation suitable to vacuum chambers has also been applied to the study of beam-induced damage to the Tevatron collimators which occurred in December 2003.

Several implementations of the continuum gas dynamics method have been used in the literature for modeling the expansion of ablation plumes. Most approaches deal with 1D or 2D Euler equations coupled to transport equations for the concentration of gas species. Extreme pressure and density gradients present computational challenges for numerical schemes and limit their applicability range. 2D approximations do not allow the study of MHD processes in ablated plumes. To deal effectively with such numerical difficulties, we have implemented surface ablation models in our 3D FronTier-MHD code (see Section 4.3.3) and applied it to the study of the expansion of laser ablation plumes in low density ambient gases. We have obtained good agreements with experiments on the expansion dynamics and internal structure of plumes [1]. We have also numerically demonstrated a strong influence of the magnetic field on the evolution and parameters of ablated plumes [3].

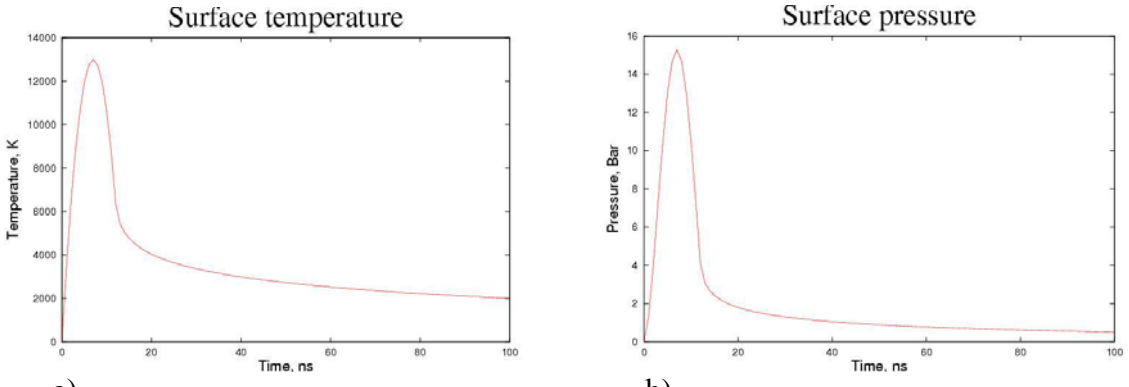

a) b)

Figure 29. Conditions on the surface of the silicon target during the laser ablation predicted by the ablation model. Evolution of the target surface temperature (a) and pressure of the ablated gas (b).

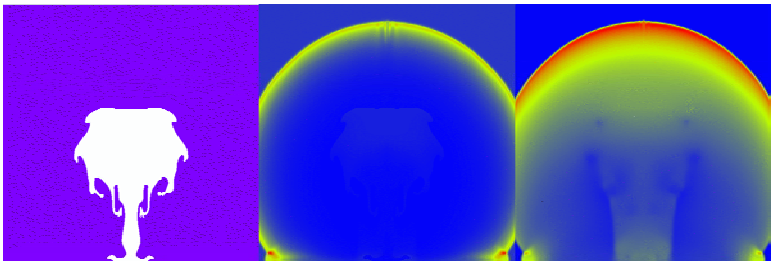

a) b) c)

Figure 30. Numerical simulation of the expansion of a laser ablation plume into background gas: a) shape of the ablated material, b) density distribution, c) pressure distribution.

References

[1] Harilal, S.S., Bindhu, C.V., Tillack, M.S., Najmabadi, F., and Gaeris, A.C. Internal structure and expansion dynamics of laser ablation plumes into ambient gas. J.Appl.Phys. **93**: 2380-2388 (2003).

[2] Knight, C. Theoretical modeling of rapid surface vaporization with back pressure. AIAA Journal **17 (5):** 519–523 (1979).

[3] Samulyak, R. and Prykarpatskyy, Y. Dynamics of laser ablation plumes in magnetic fields: modeling and simulations, Physics of Plasmas (2004). Submitted.

4.4.6 Electrodynamics Simulations: Photonic Devices and RF Cavity Design

N. D'Imperio and J. Glimm

Photonic structures have numerous applications: light emitting diodes, low loss optical devices with increased extracting capability (high Q, low volume and thin cavities, surface grating couplers), lasers, waveguides, low-loss waveguide bends, junctions, couplers and many more. Photonic crystals are a novel class of optical materials fabricated with at least two different dielectric permittivities in a periodic arrangement. They have the ability to suppress, enhance, or otherwise control the emission of light in a selected frequency range by altering the density of states. A complete photonic band gap (PBG), i.e,. a range of frequencies for which light cannot propagate through the crystal in any direction, is a spectral region where the density of states in an infinite crystal vanishes.

RF Cavities are important in accelerator design, providing the means by which the beam is accelerated using active cavities and taking measurements using passive cavities.

We have developed MAXSSIM, a parallel, scalable, finite-difference time-domain (FDTD) [1] code capable of simulating various electrodynamics problems of interest, including photonic crystals. The code can handle complex geometry, realistic initial and boundary conditions, finite size effects including absorbing boundary conditions using the Perfectly Matched Layer (PML) [2], dispersive and nonlinear media, and surface waves. Our primary focus is on the simulation of realistic experimental structures, such as waveguides, laser cavities, and frequency doublers.

Currently, we are applying our results on defect modes and localization effects to laser structures that are laterally confined by a photonic crystal and capped with Bragg reflectors longitudinally (PBG-VCSEL's). Design studies comparing PBG-VCSEL's with dielectric post VCSEL's are currently underway in collaboration with Joseph Haus and Andrew Sarangan, both of the University of Dayton.

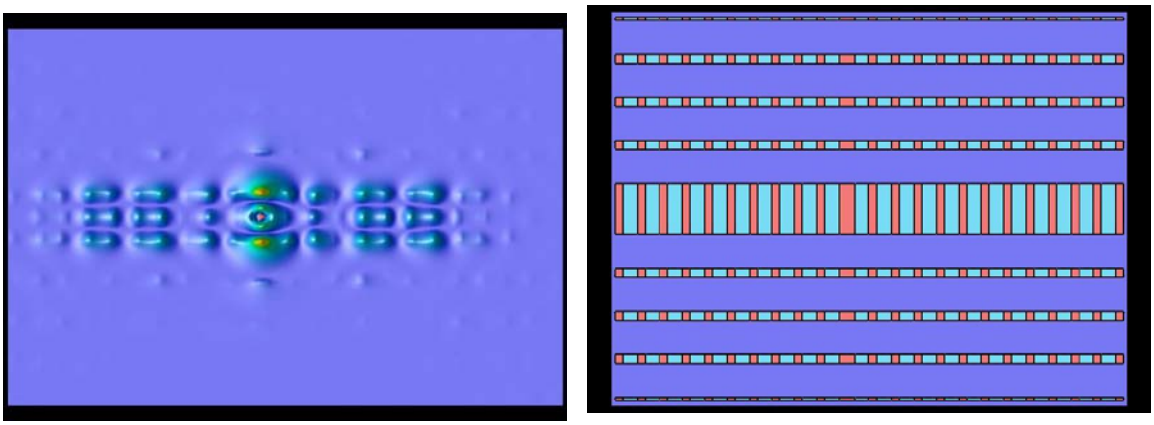

(a) (b)

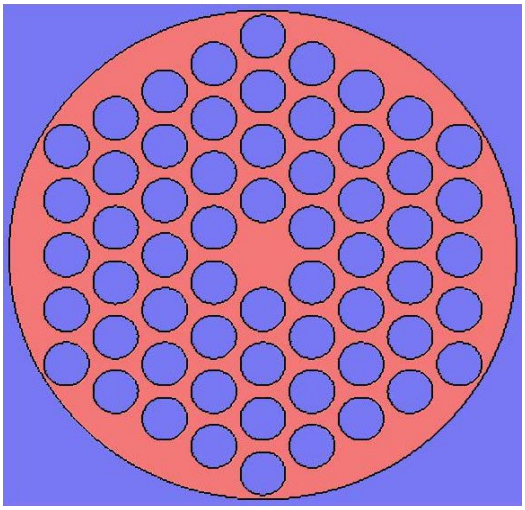

(c)

Figure 31. (a) Longitudinal slice showing the electric field energy excited by an electric dipole located in the defect layer of the VCSEL. Energy confinement due to the Photonic Crystal is very high and single mode excitation is evident. (b) Longitudinal cross section of the PBG-VCSEL. Dark blue regions indicate air, light blue and red regions are alternating Gallium Arsenide/Aluminum Arsenide dielectric layers. (c) Transverse cross section of the PBG-VCSEL illustrating the photonic crystal implemented as etched holes.

Some effort has been undertaken on applying MAXSSIM to RF Cavity modeling and design. One area of interest is studying the effects of cavities on beams as they traverse the structure. See Figure 32.

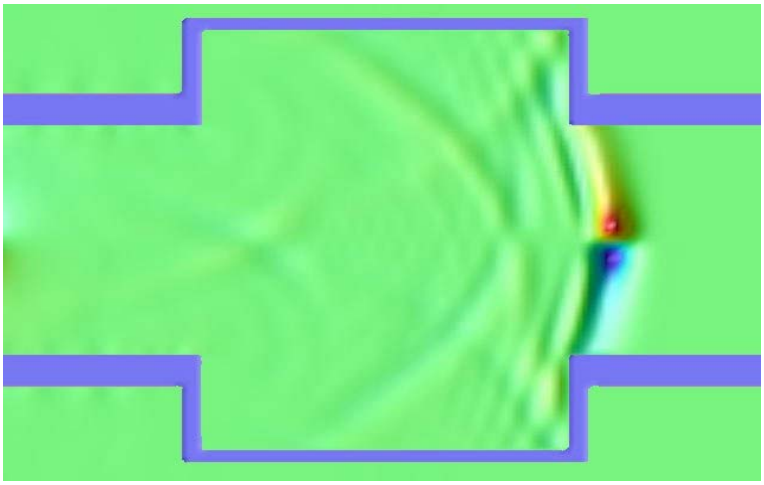

Figure 32. The y component of the electric field generated by a gaussian beam passing through a rectangular cavity with circular pipes attached. A cross section of the cavity and pipes has been superimposed on the image to more clearly show the boundaries.

References

[1] Yee, K.S. Numerical Solution of Initial Boundary Value Problems in Isotropic Media. IEEE Trans. Antennas and Propagation **14:** 302 (1996).

[2] Stojic, N., Glimm, J., Deng, Y., and Haus, J.W. Transverse magnetic defect modes in two-dimensional triangular-lattice photonic crystals. Physical Review E **64:** 1-7, Paper #056614 (2001).

[3] Smith, D.R., Dalichaouch, R., et al. J. Opt. Soc. Am. B **10:** 314 (1993).

[4] Sakoda, K. Numerical study on localized defect modes in two-dimensional triangular photonic crystals. J. Applied Physics **84:** 1210 (1998).

4.5 HIGH ENERGY AND NUCLEAR PHYSICS

New major physics facilities are central to the vitality of the nation's HENP programs. Due to their expense and complexity, simulation codes are integral to the design process. Design errors have been a major contributor to past instances of project cancellations and missed target performance. For this reason, design teams will increasingly use high performance computing, developed in national, multi-laboratory collaborations to address simulation issues in the design, operation, and control of accelerators.

4.5.1 Muon Collider Target

R. Samulyak, Y. Prykarpatskyy, and J. Glimm

In order to understand the fundamental structure of matter and energy, an advance in the energy frontier of particle accelerators is required. Advances in high energy particle physics are paced by advances in accelerator facilities. The aim of the multi institutional research group Muon Collider/Neutrino Factory Collaboration is to explore the feasibility of a high energy, high luminosity muon-muon collider [1]. For more information, visit the Muon Collider/Neutrino Factory Collaboration home page (http://www.cap.bnl.gov/mumu). However, several challenging technological problems remain to be solved in the collider design in order to achieve potential advantages of greatly increased particle energies over traditional electron-positron machines (linear colliders). One of the most important problems is to create an effective target able to generate high-flux muon beams. The need to operate high atomic number material targets in particle accelerators that will be able to withstand intense thermal shock has led to the exploration of free liquid jets as potential target candidates for the proposed Muon Collider. The target will contain a series of mercury jet pulses of about 1 cm in diameter and 30 cm in length. Each pulse will be shot at a velocity of 30-35 m/s into a 20 Tesla magnetic field at a small angle to the axis of the magnetic field. When the jet reaches the center of the magnet it will be hit with a 2 ns proton pulse. Every proton pulse will deposit about 100 J/g of energy in the mercury.

Numerical simulations of hydro and MHD processes in the target can reduce the amount of costly experiments and help with the target optimization. Such simulations present a challenging problem of computational science. They require mathematical modeling of complex flows undergoing phase transitions (cavitation) and numerical tools for solving MHD equations in complex geometries. Our numerical studies have been performed using FronTier-MHD, a magnetohydrodynamic extension of the front tracking hydro code FronTier (for more details, see Section 4.3.3). Numerical simulations of the Muon Collider target have already achieved important results. Some analytical estimates and numerical studies of the evolution of conducting liquid jets and the mercury target in particular as they enter a strong nonuniform magnetic field were obtained in [7]. Numerical simulations of the interaction of the mercury jet with a proton pulse have shown that strong waves caused by the proton energy deposition lead to surface instabilities and the breakup of the jet [4,6]. Simulations agree with recent experiments carried out at BNL Alternating Gradient Synchrotron and CERN [2,3]. It has also been shown that the magnetic field tends to stabilize the Richtmyer-Meshkov type instability in the mercury jet [4.6]. Since cavitation plays an important role in the hydrodynamics of the target, different cavitation models have been developed and validated using theoretical predictions and experimental results [4,5] (see also Section 4.4.4). They have also been used for the study of some hydrodynamic aspects of the cavitation induced erosion in the mercury target for the Spallation Neutron Source (see Section 4.5.4).

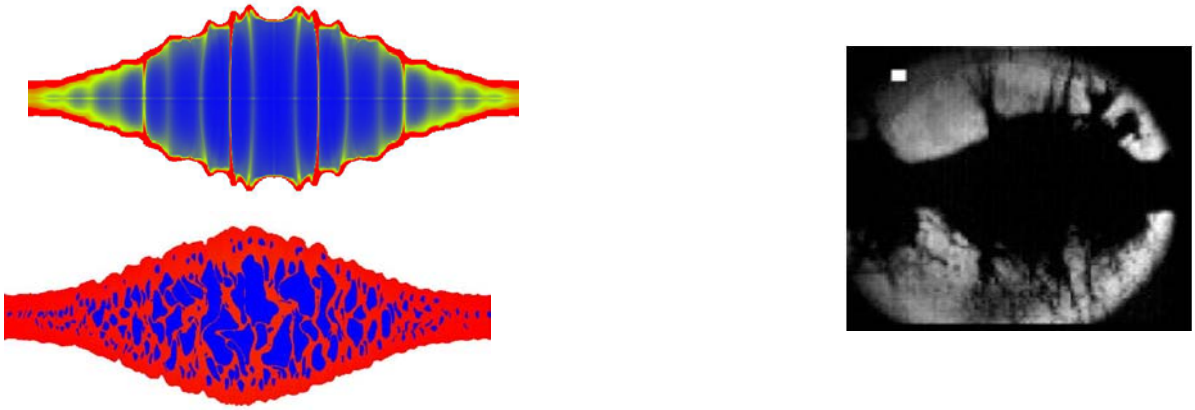

a) b)

Figure 33. Comparison of cavitation simulations in the mercury target obtained using the homogeneous and direct numerical simulation methods, and experimental results. a) Density distribution in the mercury jet obtained using the homogeneous EOS model (top) and direct numerical simulation of cavitation bubbles (bottom). b) Experimental image of the mercury jet.

The current work is in the area of modeling of complex flows undergoing phase transitions and the development of improved numerical algorithms for the direct numerical simulation of the cavitation and MHD elliptic solvers. Specifically, we have been working on the finite volume discretization of elliptic equations in complex geometries, Riemann solver for the phase boundary, coupling cavitation models with MHD solvers, and large-scale, 3D numerical simulations of hydro and MHD processes in the Muon Collider target.

References

[1] Alsharoa, M. et al. Recent progress in neutrino factory and muon collider research within the Muon Collaboration. Phys. Rev. Special Topics - Accelerators and Beams **6(8):** 52 pages (2003).

[2] Fabich, A. and Lettry, J. Experimental Observation of Proton-Induced Shocks and Magneto-Fluid-Dynamics in Liquid Metal, In Proc. *NuFact* 01, NIM A, 2001.

[3] Kirk, H. et al. Target studies with BNL E951 at the AGS, Particles and Accelerators 2001. June 18-22, 2001, Chicago IL.

[4] Samulyak, R. and Prykarpatskyy, Y. Richtmyer-Meshkov instability in liquid metal flows: influence of cavitation and magnetic fields. Mathematics and Computers in Simulations **65:** 431-446 (2004).

[5] Samulyak, R., Lu, T., Prykarpatskyy, Y., Glimm, J., Xu, Z., and Kim, M.-N. Comparison of direct and homogeneous numerical approaches to cavitation modeling. Int. J.for Multiscale Comp. Eng. (2004). Submitted.

[6] Samulyak, R., Glimm, J., Oh, W., Kirk, H., and McDonald, K. Numerical simulation of free surface MHD flows: Richtmyer - Meshkov instability and applications. Lecture Notes in Comp. Sci. **2667:** 558-567 (2003), Springer-Verlag, Berlin - Heidelberg, 2003.

[7] Samulyak, R. Numerical simulation of hydro- and magnetohydrodynamic processes in the Muon Collider target. Lecture Notes in Comp. Sci. **2331:** 391-400 (2002), Springer-Verlag, Berlin - Heidelberg, 2002.

4.5.2 Modeling of Wake Fields and Impedances in Accelerators

R. Samulyak

The electromagnetic interaction of an intensive charged particle beam with its vacuum chamber surroundings in an accelerator plays an important role for the beam dynamics and collective beam instabilities. Wake fields, generated by a moving particle in the accelerator pipe and objects such as RF cavities, bellows, stripline monitors etc., affect the motion of particles in the tail part of the beam causing the parasitic loss, beam energy spread, and instabilities. The effect of wake fields is usually of the same order of magnitude as the space charge effect. While the space charge forces approach zero in the ultrarelativistic limit, wake fields remain finite for an ultrarelativistic beam due to resistivity of the accelerator walls and non-smoothness of the chamber (existence of RF cavities, bellows etc.). The effect of wake fields is an increasingly important issue since operating regimes are continually moving towards higher currents and smaller bunches. To avoid collective beam instabilities that limit the accelerator performance, an accurate numerical modeling of wake fields and their interaction with the beam is necessary.

In the traditional approach for including wake field forces in an accelerator code, the total impedance budget for the accelerator ring is calculated or experimentally measured and the corresponding forces are applied to tracked particles once per beam turn. Such a cumulative force approach is not sufficient for the simulation of beam instabilities caused by wake fields. It is less accurate than the 3D computation of the space charge which has already been developed in advanced accelerator modeling codes including the MaryLie/Impact code [2]. We have developed a model which accounts for the fine structure of particle beams and distributes wake fields in the accelerator chamber. The corresponding theoretical model is based on the expansion of the particle beam in terms of the multipole moments and the notion of the wake function which allows to eliminate the complex temporal behavior of the electromagnetic field between the incident charge creating the wake field and the test charge. The wake function describes the response of the accelerator chamber element to a delta-functional pulse carrying m-th moment. Wake functions are independent of the beam properties and defined totally by properties of the accelerator chamber. Therefore the longitudinal and transverse wake field forces, caused by a particle carrying the moment I_m, integrated over a length L and acting on a test charge e can be represented in terms of the longitudinal and transverse wake functions, $W_m^{'}(z)$ and $W_m(z)$:

$$\int_{-L/2}^{L/2} ds\, \vec{F}_{\parallel} = -eI_m W_m^{'}(z)\, r^m \hat{\mathbf{s}} \cos m\theta,$$

$$\int_{-L/2}^{L/2} ds\, \vec{F}_{\perp} = -eI_m W_m(z)\, m r^{m-1} \left(\hat{\mathbf{r}} \cos m\theta - \hat{\boldsymbol{\theta}} \sin m\theta \right).$$

The wake field algorithm is coded as a parallel Fortran 90 module which performs the charge deposition of macroparticle beams on a 3D grid, expansion of the corresponding charge distribution into miltipole moments, computation of wake functions and wake field forces, and interpolation of the wake field forces from the grid to macroparticles. The module has been implemented in MaryLie/Impact code and used for the study of wake field effects on the beam dynamics in simple focusing-defocusing channels and circular accelerators. In the current numerical implementation, most of the accelerator chamber elements (resistive pipe, RF cavity etc.) have associated analytical wake field models valid under certain approximations [1]. Analytical wake field models are beneficial for the study of long-range wake fields and their multiturn effect on the beam dynamics in circular accelerators. To study wake field effects in accelerator elements which can not be accurately approximated by analytical models, wake functions in a tabular format can also be used. The corresponding data can be obtained through accurate numerical solutions of the full Maxwell system of equations using commercial (MAFIA) or public domain electromagnetic codes.

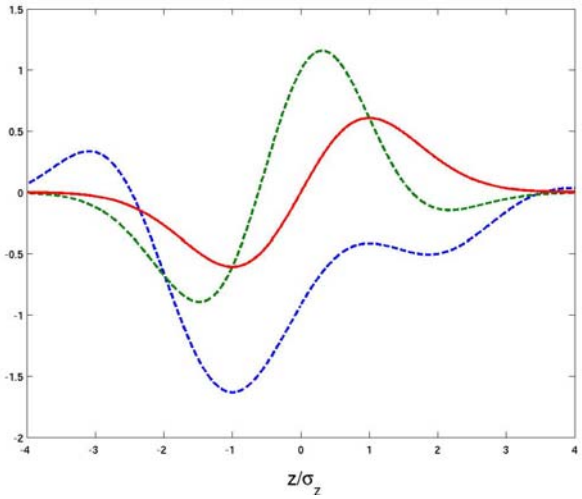

Figure 34. Energy spread due to the longitudinal space charge forces (red line, in units of $q/\gamma^2\sigma_z^2$), zero-mode resistive wake fields (blue line, in units of $\frac{q}{b\sigma_z^{3/2}}\sqrt{\frac{c}{2\pi\sigma}}$), and the resonator model wake fields (green line, in units of $\frac{qR_s c^2}{Q\omega_R\sigma_z^2}$) for a short bunch with the Gaussian longitudinal distribution and a uniform disk transverse distribution.

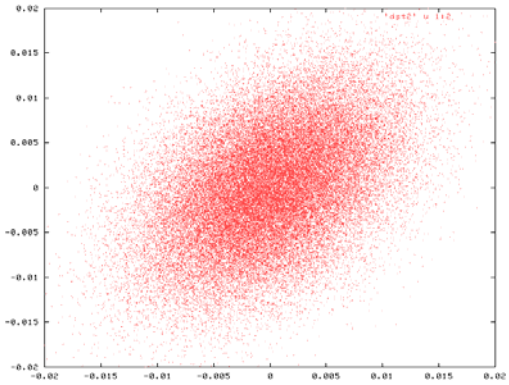

Figure 35. Dipole type distortion of a particle bunch due to the first mode resistive wall wake fields.

References

[1] Chao, A.W., and Tinger, M. *Handbook on Accelerator Physics and Engineering*. World Scientific, 1998.

[2] Ryne, R., Qiang, J., Dragt, A., Habib, S., Mottershead, T., Neri, F., Samulyak, R., and Walstrom, P. MaryLie/IMPACT: a parallel beam dynamics code with space charge. In: *Proc. of the Computational Accelerator Physics Conference, Oct. 15-18, 2002.*

4.5.3 Unified Accelerator Library: SIMBAD

N. D'Imperio and A. Luccio

Working in collaboration with computational physicists at BNL's Collider Accelerator Department, we have continued development on a Particle-in-Cell (PIC) [1] code to model collective beam effects in two and three dimensions. The code was formerly known as ORBIT and is being integrated into the Unified Accelerator Libraries (UAL) [2] as the SIMBAD component for the modeling of space charge.

UAL provides a framework in which the tracking of particles takes place by pushing a "bunch" of macropartcles through a lattice using the TEAPOT code, which has also been integrated in UAL. Space charge is calculated separately using SIMBAD. Once all particles have reached a certain location, their charge density is calculated by binning to a grid. The potential Φ is found by solving the Poisson equation with the perfectly conducting wall boundary conditions:

$$\Delta\Phi = -\rho/\varepsilon,\ \rho_{wall}(x,y,z) = 0.$$

Space charge force components (with coefficients to account for both the electrostatic and magnetic action) are calculated as derivatives of the potential and applied to each macro particle in the transverse direction. Longitudinal space charge is calculated by binning the particles longitudinally and following the formalism presented in [1]. In a ring with long longitudinal bunches, the transverse motion can be uncoupled from the longitudinal, and the Poisson equation can be solved in parallel in many longitudinal beam segments.

The parallelization of SIMBAD is implemented differently in 2-d as opposed to 3-d. In 2-d, the parallelization is implemented by dividing the macro particles among the processes and collectively calculating the forces on each mesh. In 3-d, each process takes a number of longitudinal slices and calculates the space charge forces only within its own slices. This parallelization requires load balancing that considers both the number of particles and the number of slices. This is accomplished using a genetic algorithm [3]. Figure 36 shows parallel decomposition of the bunch and the resulting division of the beam.

The code was used to model high intensity beams in the Alternating Gradient Synchrotron at BNL to study its suitability as a proton driver [3]. Figure 37 shows the rms transverse emittance vs. turn number. The space charge couples the two transverse coordinates while the two emittances reach a steady state after some turns. A Montague resonance is observed.

UAL is being ported to run on the Blue Gene Light and QCDOC supercomputers where beam-beam interaction will be simulated.

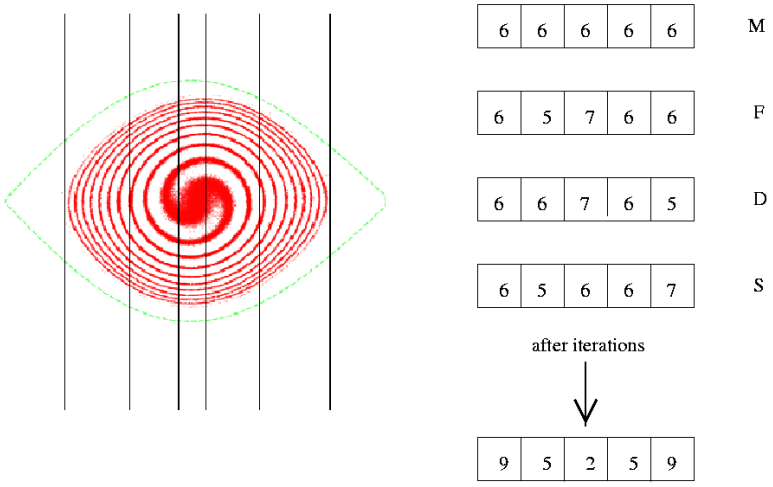

Figure 36. Bunch decomposition and load balancing. (a) A bunch of macro particles in an RF bucket with accompanying lines to indicate the boundaries for each of 5 processes. (b) Genetic algorithm produces an optimal balance between number of particles per process and number of slices per process.

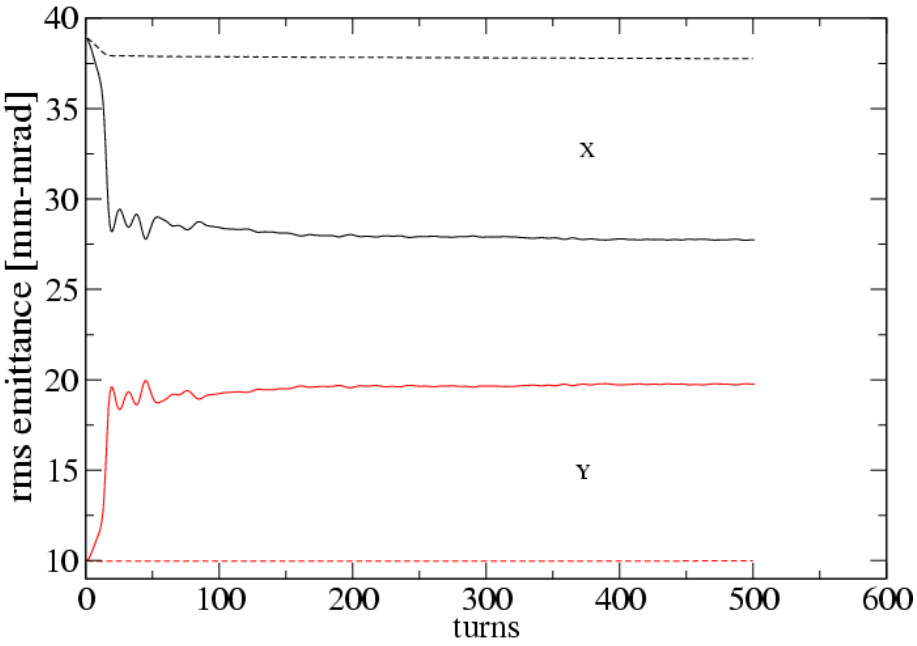

Figure 37. Emittance vs. turns for the AGS at low and high intensity. The dashed lines are low intensity, solid lines indicate high intensity. Transverse coupling is very noticeable at high intensity.

References

[1] Chao, A.W. *Physics of Collective Beam Instabilities in High Energy Accelerators*. Wiley, 1993.

[2] Malitsky, N. and Talman, R. Unified Accelerator Libraries. In *Computational Accelerator Physics,* AIP Conference Proceedings 391, J.J. Bisognano and A.A. Mondelli, Eds., pp. 337-342 (1997).

[3] Luccio, A. and D'Imperio, N. Simulation of the AGS as a proton driver. ICFA Beam Dynamics Mini Workshop on Space Charge Simulation, Oxford, UK, Trinity College, April 2-4, 2003, www-bd.fnal/icfa/workshops (2003).

4.5.4 Spallation Neutron Source Target

R. Samulyak, T. Lu, and Y. Prykarpatskyy

The Spallation Neutron Source (SNS) is an accelerator-based neutron source being built in Oak Ridge, Tennessee, by the U.S. Department of Energy (http://www.sns.gov). The SNS will provide the most intense pulsed neutron beams in the world for scientific research and industrial development.

The proposed liquid mercury target design for the Spallation Neutron Source (see Figure 38) includes a main flow region inside a stainless steel structure where mercury enters from the sides, flows around a baffle into the proton beam path, and exits out the center. A cooling jacket that wraps from bottom to top around the target is used to cool the target window through which the proton beam enters. The stainless steel target structure is approximately 0.5 x 0.4 x 0.15 m^3.

One of the most important issues associated with using liquid metals as targets for pulsed proton beams is withstanding the loads caused by the rapid pressure increase resulting from the intense heating of the liquid metal from a single pulse of protons. This heating occurs essentially instantaneously compared to acoustic time scales; therefore, the mercury undergoes a large pressure increase. In addition to a set of difficult engineering problems associated, for instance, with the design of windows able to withstand large thermal gradients and shocks, recent experiments with an SNS target prototype uncovered yet another problem critical to the target lifetime. They showed pitting of stainless steel surfaces that were in contact with mercury subject to large pressure pulses induced by the collapse of cavitation bubbles [1]. Due to the cavitation induced erosion, it will be necessary to replace the target after two weeks of operation at frequency 60 Hz of a 1 MW proton pulse. To extend the target lifetime, future research efforts will be concentrated in two areas, each of which should lead to reduction of the erosion damage:

- Evaluation of cavitation resistant materials and coatings.
- Investigation of mitigation techniques such as introduction of non-dissolvable bubbles into the system.

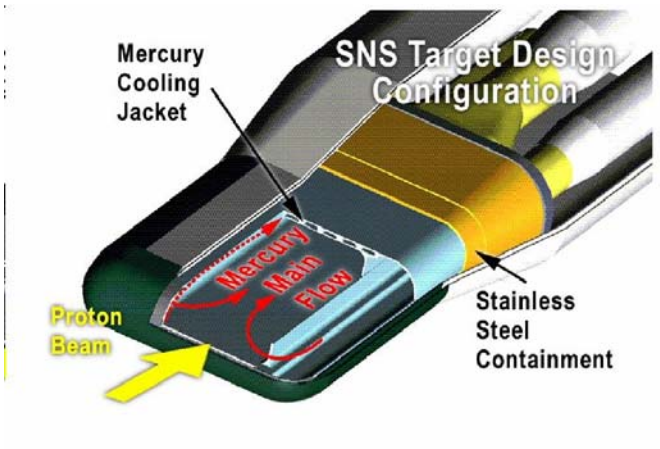

Figure 38. SNS mercury target design.

We have been working on the modeling of cavitation and bubbly fluids and the numerical simulation of hydrodynamic processes related to cavitation induced erosion. The main goal of the research is to explore possible ways of reducing the cavitation and extending the target lifetime. In our studies, we collaborate with SNS targetry research group. The areas of research include:

- Development of new equation of state models for the cavitation dynamics and flow of liquids containing non-dissolvable gas bubbles (See Section 4.4.4 for more details). The first class of models is based on the direct tracking of gas-liquid interfaces in multiphase flows (Figure 33). Such an interface tracking is a key feature of our hydrodynamic code FronTier. The second class of models uses a homogeneous description of a multiphase system as a pseudofluid [2].
- Global numerical simulations of the wave dynamics in the target container using the FronTier and ABAQUS codes and new EOS modules. It includes benchmarking with experimental data on the SNS target strain response to beam induced pressure pulses, numerical studies of the geometric effects capable of reducing reflected tensile waves, and optimization of the target container shape.
- Evaluation through numerical simulations the efficiency of mitigation techniques which use layers of non-dissolvable gas bubbles near target windows and gas bubbles in the bulk mercury. We have been working on numerical simulations of the interaction of strong waves with bubbly flows using the homogeneous equation of state models and direct numerical simulations of the bubble dynamics based on FronTier's interface tracking capabilities.
- Numerical studies using FronTier's interface tracking technique of the hydro jet arising in a cavity collapse and its interaction with the wall.

We have applied the direct numerical simulation technique for bubbly fluids to the study of pressure mitigation through the injection of non-dissolvable gas bubbles near the target front window. We have found that while the bubbly layer indeed causes a significant reduction of pressure during 200 microseconds, large transient pressure oscillations may exist for a short period of time (< 100 microseconds) after the proton beam energy deposition (see Figure 39). Such transient oscillations, which are absent in the pure mercury, can at some conditions lead to an enhanced cavitation on the front flange. We have been working on the analysis of cavitation of mercury and the collapse of cavitation bubbles in the presence of rapid pressure oscillations. The

preliminary results are encouraging: they show that distractive cavitation does not develop at certain parameters of the bubbly mixture. We will continue numerical studies of the bubbly layer mitigation technique in order to perform parameter optimization and assist the next series of experimental studies.

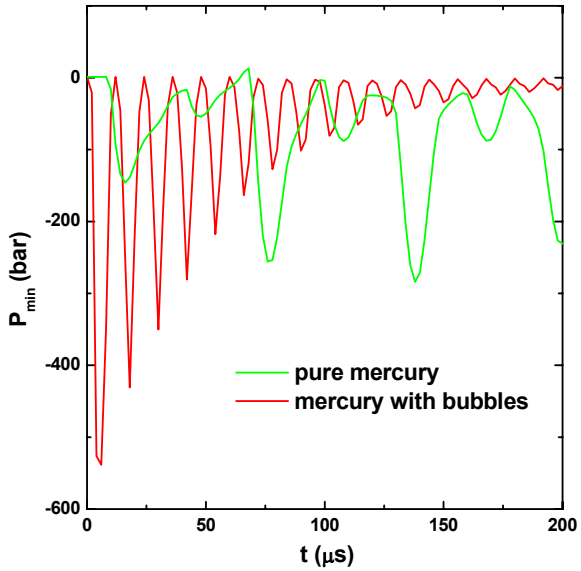

Figure 39. Numerical simulation of the dynamics of waves in the SNS target using direct numerical technique for multiphase flows. Minimum value of the pressure on the target flange for pure mercury (green line) and for mercury containing a layer of gas bubbles (red line).

References

[1] Status Report on Mercury Target Related Issues, SNS-101060100-TR0006-R00, July 2002.

[2] Samulyak, R., Lu, T., and Prykarpatskyy, Y. Direct and homogeneous numerical approaches to multiphase flows. Lecture Notes in Comp. Sci. **3039:** 653-660 (2004), Springer-Verlag, Berlin - Heidelberg.

4.5.5 Grid Computing: MonALISA

Development and Use of MonALISA High Level Monitoring Services for the STAR Unified Meta-Scheduler

E. Efstathiadis, L. Hajdu, J. Lauret, and I. Legrand (CalTech)

As a Particle Physics Data Grid (PPDG) cross team-project we study, develop, implement and evaluate a set of tools that allow Meta-Schedulers to take advantage of a consistent set of shared information (such as information needed for complex decision making mechanisms) across both local and Grid Resource Management Systems. We demonstrate the usefulness of such tools within the MonALISA monitoring framework and the STAR Unified Meta-Scheduler.

We define the requirements and schema by which one can consistently provide queue attributes for the most common batch systems and evaluate the best scalable and lightweight approach to access the monitored parameters from a client perspective and, in particular, the feasibility of accessing

real-time and aggregate information. Client programs are envisioned to function in a non-centralized, fault tolerant fashion.

We believe that such developments could highly benefit Grid laboratory efforts such as the Grid3+ and the Open Science Grid (OSG).

The MonALISA (Monitoring Agents in A Large Integrated Services Architecture) system provides a distributed monitoring service. It is based on a scalable Dynamic Distributed Services Architecture (DDSA) that is implemented using JINI/JAVA and WSDL/SOAP technologies. The scalability of the system derives from the use of autonomous multi-threaded station servers to host a variety of loosely coupled, self-describing, dynamic services, the ability of each service to register itself and then to be discovered and used by other services or clients that require such information, and the ability of all services and clients subscribing to a set of events (state changes) in the system to be notified automatically. The framework integrates several existing monitoring tools and procedures to collect parameters describing computational nodes, applications and network performance. It has built-in SNMP support and network-performance monitoring algorithms that enable it to monitor end-to-end network performance as well as the performance and state of site facilities in a Grid.

The core of the MonALISA monitoring service is based on a multithreaded system (the monitoring service) used to perform the many data collection tasks in parallel, independently. It is designed to easily integrate existing monitoring tools and procedures and to provide this information in a dynamic, self-describing way to any other services or clients. MonALISA services are organized in groups and their group attribute is used for registration and discovery. Each service registers with a set of JINI Lookup Discovery Service (LUS), as a member of a group, and having a set of attributes. The LUSs are also JINI services and may be registered with other LUSs resulting in a distributed and reliable network for registration of services. Services also provide the code base for the proxies that other services or clients will need to instantiate for using it.

A generic framework for building pseudo-clients for the MonALISA services was developed. This has been used for creating dedicated web service repositories with selected information from specific groups of monitoring services. The pseudo-clients use the same LUSs approach to find all the active MonALISA services from a specified set of groups and subscribe to these services with a list of predicates and filters. These predicates or filters specify the information the pseudo-client wants to collect from all the services. Pseudo-clients store received values from the running services in a local MySQL database. A Tomcat based servlet engine is used to provide a flexible way to present global data and to construct on the fly graphical charts for current or customized historical values, on demand. Multiple Web Repositories can easily be created to globally describe the services running in a distributed environment.

Queue monitoring data collected using custom MonALISA modules at each site are cached locally using pseudo-clients with fail-over capabilities. This way the monitoring data from all services that have joined a group are available to policies implemented into the Meta-Scheduler that choose the appropriate queue for the submitted job.

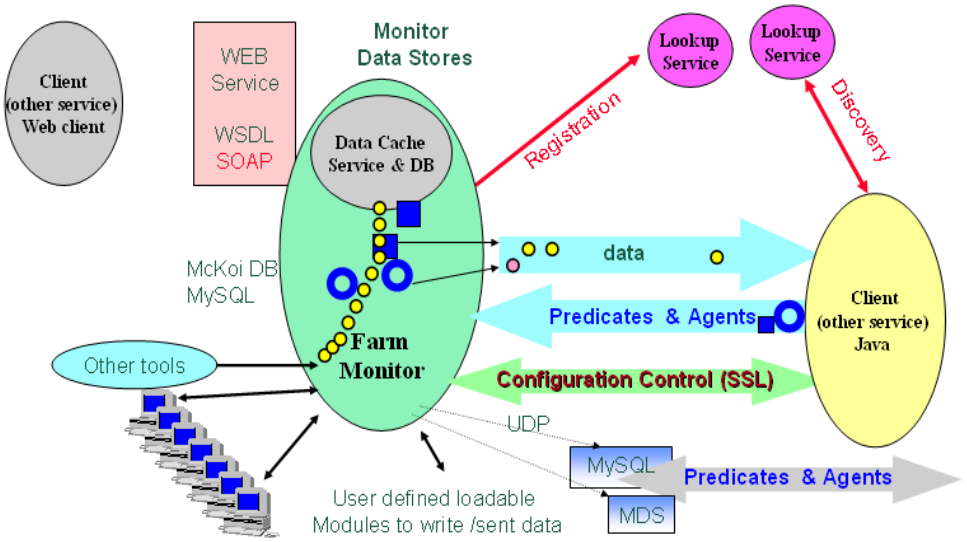

Figure 40. The MonALISA monitoring service.

References

[1] Efstathiadis, E. et al. Proceedings of the Computing in High Energy Physics (CHEP) 2004 conference, Interlaken, Switzerland, Sept. 26 - Oct. 1st, 2004 (to be published).

[2] http://www.ivdgl.org/documents/document_server/uploaded_documents/doc--998--iVDGL_Star_monitoring.ppt

[3] http://indico.cern.ch/getFile.py/access?contribId=393&sessionId=7&resId=0&materialId=slides&confId=0